Molecular Therapy
Original Article

IL-18 metabolically reprograms CAR-expressing natural killer T cells and enhances their antitumor activity

Gabriel A. Barragán Bravo,[1] David A. de la Cerda,[1] Elisa Landoni,[2] Kshiti Dholakia,[1] Piotr Humeniuk,[1] Leidy D. Caraballo Galva,[1] Ying Wang,[1] Gengwen Tian,[1] Boning Yang,[1] Linjie Guo,[1] Michael S. Wood,[1] Xavier Rios,[1] Xin Xu,[1] Amy N. Courtney,[1] Erica J. Di Pierro,[1] Joan Jacob,[1] Yi-Han Li,[1] Akshaya Adaikkalavan,[1] Norihiro Watanabe,[1,3] Sufeng Mao,[4] George Miles,[4,5] Gianpietro Dotti,[2] and Leonid S. Metelitsa[1,3]

[1]Center for Advanced Innate Cell Therapy, Texas Children's Cancer Center, Department of Pediatrics, Baylor College of Medicine, Houston, TX 77030, USA; [2]Lineberger Comprehensive Cancer Center, University of North Carolina, Chapel Hill, NC 27599, USA; [3]Center for Cell and Gene Therapy, Baylor College of Medicine, Houston, TX 77030, USA; [4]Lester and Sue Smith Breast Center, Baylor College of Medicine, Houston, TX 77030, USA; [5]Department of Molecular and Human Genetics, Baylor College of Medicine, Houston, TX 77030, USA

Invariant natural killer T cells (NKTs) have intrinsic antitumor properties that make them promising candidates for chimeric antigen receptor (CAR) immunotherapies. Transgenic cytokine expression can enhance cellular therapy potency, and we hypothesized that co-expressing interleukin-18 (IL-18) alone or with IL-15 would boost CAR-NKT therapeutic potential. To test this, we generated retroviral constructs expressing IL-15 and/or IL-18 with an inducible caspase-9 safety switch and co-transduced them with a GD2-specific CAR into human NKTs. Co-expression of IL-18 or IL-15/IL-18 increased CAR-NKT cytotoxicity, proliferation, and cytokine secretion *in vitro* compared to IL-15 alone. IL-18 also enhanced GPC3.CAR and CD19.CAR NKT activity against hepatocellular carcinoma and B cell leukemia cells, respectively. In a metastatic neuroblastoma model, IL-18-expressing GD2.CAR-NKTs controlled tumors more effectively than IL-15-only cells, but mice in the IL-15/IL-18 group developed severe toxicities not observed in the IL-18-only group. Mechanistically, IL-18 induced a transcriptional program distinct from IL-15, marked by lower exhaustion signatures and enrichment of metabolic pathways. Finally, targeted metabolomics showed that IL-18 drives broad metabolic reprogramming in CAR-NKTs including increased oxidative phosphorylation, glycolysis, glutaminolysis, and purine metabolism. These findings support the use of IL-18 in developing the next generation of cytokine-armed CAR-NKT cancer immunotherapies.

INTRODUCTION

Despite significant progress in treating hematologic malignancies, T cells expressing chimeric antigen receptors (CARs) have generated few clinical responses in patients with solid tumors to date.[1] This is partially because CAR-T cells do not localize well to tumor sites and do not have the metabolic fitness to avoid rapid exhaustion and loss of function in the immunosuppressive solid tumor microenvironment (TME).[2] Strategies to enhance the trafficking of CAR-T cells to tumors and boost therapeutic effector cell function in the TME are urgently needed to achieve durable control of solid tumors while managing toxicity.

Compared to conventional T cells, several types of innate or innate-like lymphocytes including natural killer (NK), γ/δ T, and CD1d-restricted invariant natural killer T cells (NKTs) have intrinsic antitumor properties including the ability to effectively home to tumor sites.[3–6] These unconventional effectors can also be redirected using tumor-antigen-specific CARs to effectively target solid malignancies.[7–11] We recently found that despite showing similar levels of cytotoxicity to CAR-T cells *in vitro*, CAR-NKTs exert significantly more potent *in vivo* antitumor activity in multiple solid tumor models.[12] NKTs can also mediate indirect antitumor activity by killing or inhibiting M2-like tumor-associated macrophages (TAMs) in a CD1d-dependent manner[13–15] and through $CD8^+$ T cell cross-priming.[12,16] In patients, NKT infiltration into primary tumors has been associated with improved outcomes in children[3] and adults[17] with cancer. These properties make NKTs a promising cellular platform for CAR-redirected cancer immunotherapy.[16,18–23]

Neuroblastoma (NB) is a common extracranial solid tumor of childhood, and patients with high-risk/relapsed disease have a 5-year survival rate of between 20% and 50%.[24,25] The GD2 ganglioside is expressed at high levels in NB cells and minimally expressed in normal tissues, making it a suitable target for GD2-specific

Received 18 April 2025; accepted 7 January 2026;
https://doi.org/10.1016/j.ymthe.2026.01.001.

Correspondence: Leonid S. Metelitsa, Center for Advanced Innate Cell Therapy, Texas Children's Cancer Center, Department of Pediatrics, Baylor College of Medicine, Houston, TX 77030, USA.
E-mail: lsmeteli@texaschildrens.org

Please cite this article in press as: Barragán Bravo et al., IL-18 metabolically reprograms CAR-expressing natural killer T cells and enhances their antitumor activity, Molecular Therapy (2026), https://doi.org/10.1016/j.ymthe.2026.01.001

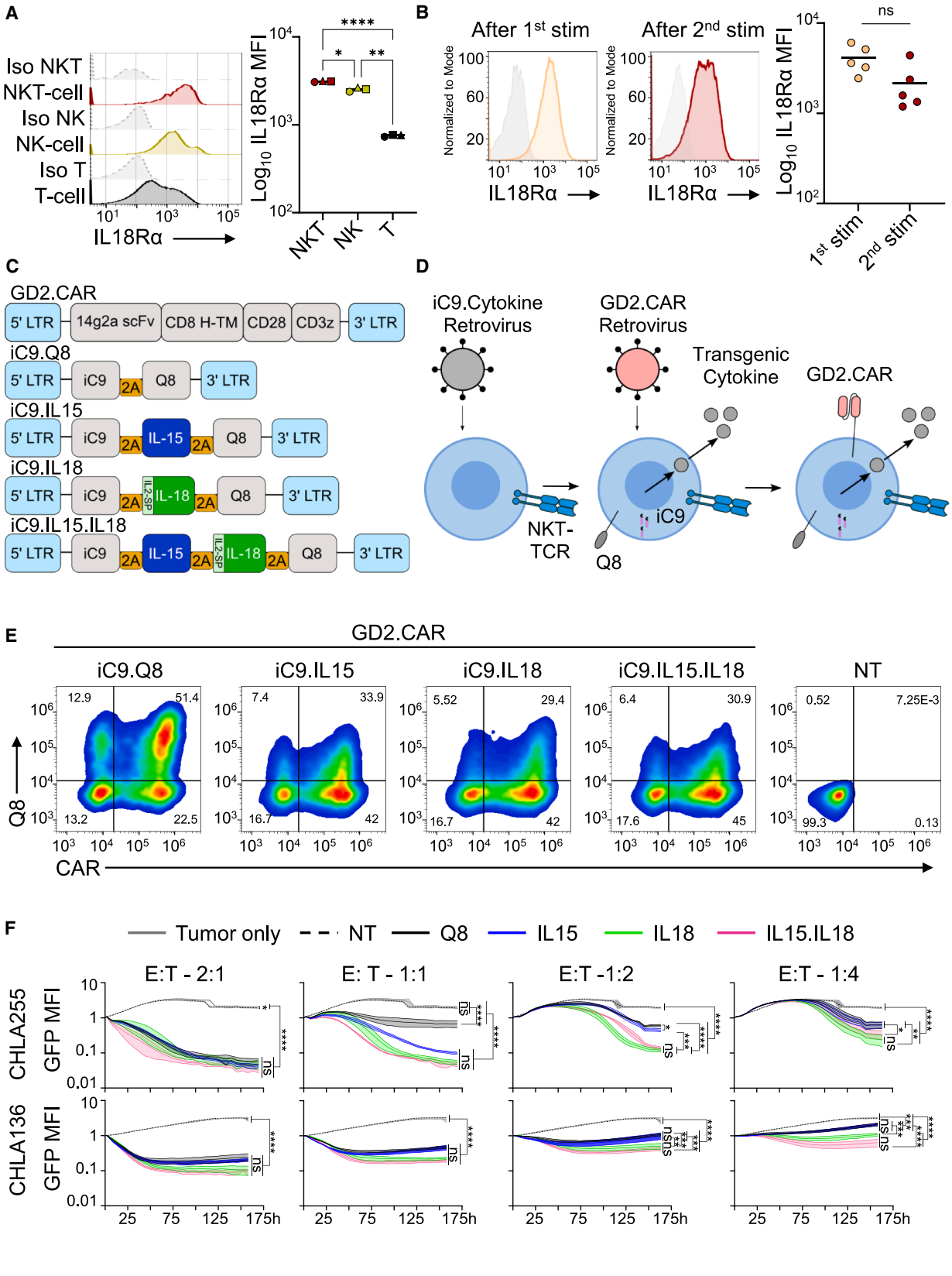

(legend on next page)

Please cite this article in press as: Barragán Bravo et al., IL-18 metabolically reprograms CAR-expressing natural killer T cells and enhances their antitumor activity, Molecular Therapy (2026), https://doi.org/10.1016/j.ymthe.2026.01.001

immunotherapy with two Food and Drug Administration-approved anti-GD2 monoclonal antibodies now available.[26,27] In the cellular immunotherapy space, several early-stage clinical trials testing GD2-specific CAR-T cells[28,29] and NKTs[30] have demonstrated safety and evidence of antitumor activity. On the GINAKIT2 trial, NKTs were engineered to co-express a GD2.CAR and IL-15, a cytokine that has been shown to support NKT and CAR-NKT persistence and antitumor activity in preclinical tumor models.[31] Beyond IL-15, the membrane-bound form of proinflammatory cytokine IL-12 has been shown to potently enhance GD2.CAR-NKT persistence and antitumor activity in xenogeneic tumor models.[32] Like IL-12, IL-18 is a proinflammatory cytokine that induces effector programs in T and NK cells[33] and stimulates interferon-γ (IFN-γ) production by and antitumor activity of murine NKTs.[34,35] IL-18 has already been shown to enhance CAR-T cell antitumor potential,[36–41] providing rationale for ongoing phase 1 trials evaluating IL-18-armed CD19.CAR-T, GD2.CAR-T, and CD371.CAR-T cells in patients with relapsed/refractory lymphomas (NCT04684563),[42] GD2-positive solid tumors (WWU19_0008), and refractory acute myeloid leukemia (NCT06017258),[43] respectively.

Here, we studied the impact of IL-18 expression on human NKTs and CAR-NKTs to determine the therapeutic utility of this cytokine in this unique effector subset. We report that freshly isolated primary human NKTs exhibited a higher level of IL-18 receptor α (IL18Rα) expression than NK and T cells from the same donors, and that IL-18 more potently enhanced CAR-NKT *in vivo* antitumor activity than IL-15 without increasing toxicity. Mechanistically, we demonstrated that IL-18 reprograms NKT metabolism, leading to improved functional fitness and resistance to exhaustion. In all, our results suggest that IL-18 expression is a promising strategy to improve the therapeutic potential of CAR-NKTs for neuroblastoma and, potentially, other solid tumors.

RESULTS

Generation of CAR-NKTs co-expressing IL-18 and/or IL-15 with an inducible caspase-9 safety switch

While IL18Rα expression has been demonstrated in cord-blood-expanded $CD4^+$ NKTs and adult healthy donor NKTs,[44,45] a comparison of IL18Rα expression levels in NKTs versus other lymphocyte subsets has not been performed. To address this, we measured IL18Rα expression in freshly isolated peripheral blood mononuclear cells (PBMCs) by flow cytometry. Interestingly, NKTs showed significantly higher IL18Rα levels than both T and NK cells (Figure 1A), suggesting that NKTs are responsive to IL-18. Additionally, IL18Rα expression was maintained at a high level in NKTs following both primary and secondary stimulations with αGalCer-loaded antigen-presenting cells (Figure 1B).

Next, to explore the impact of IL-18 expression in CAR-NKTs versus clinically tested IL-15, we generated retroviral constructs encoding IL-18 and/or IL-15, the inducible caspase-9 (iC9) safety switch,[46] and the Q8 transduction marker (Figure 1C).[47] In these constructs, the IL-18 pro-peptide was replaced with the IL-2 signal peptide sequence to ensure production of biologically active and secreted IL-18.[16] NKTs were isolated from healthy donor PBMCs and expanded as previously described,[48] followed by transduction with iC9.IL15, iC9.IL18, iC9.IL15.IL18, or iC9.Q8 control and the GD2.CAR construct 24 h later (Figure 1D). The cells were then re-stimulated and cultured in the presence of IL-2 for 9–12 days, and transduction rate and NKT purity were assessed by flow cytometry (Figures 1E and S1A). Co-expression of the iC9.IL18 or iC9.IL15.IL18 constructs affected NKT proliferation minimally during manufacturing when compared to cells expressing iC9.Q8 or iC9.IL15 (Figure S1B), and NKTs expressing these constructs secreted their respective transgenic cytokines after stimulation with NB tumor cells (Figure S1C). We confirmed activation of IL-15 signaling using intracellular staining for phosphorylated STAT5 and IL-18 signaling using a nuclear factor κB (NF-κB) reporter construct (Figures S1D and S1E).[49,50] Next, we evaluated the phenotype of CAR-NKTs expressing iC9.cytokine constructs by flow cytometry (Figure S1F). We found that IL-18 expression did not significantly impact the percentage of CAR-NKTs positive for central memory marker CD62L[51] compared to iC9.Q8 and iC9.IL15 populations and led to a minor but significant increase in the proportion of $CD4^+$ NKTs. iC9.IL18 CAR-NKTs expressed higher levels of activation/exhaustion markers CD39, LAG3, TIGIT, and TIM3 but not PD1 compared to iC9.Q8 and iC9.IL15 cells. Similar phenotypic trends were observed in iC9.IL15.IL18 CAR-NKTs. We also found minimal changes in the expression of several chemokine receptors across all groups after manufacturing (Figure S1G). These results suggest that IL-18 expression leads CAR-NKTs to exhibit an

Figure 1. Generation of CAR-NKTs co-expressing IL-15, IL-18, or IL-15/IL-18 with the iC9 safety switch

(A) Flow-cytometry histograms depicting IL18Rα expression in PBMC cell subsets from a healthy donor (left). Summary data of IL18Rα expression in PBMCs from $n = 3$ healthy donors (right). Mean is shown. $^*p < 0.05$, $^{**}p < 0.01$, $^{****}p < 0.0001$, paired one-way ANOVA. (B) Flow-cytometry histograms depicting IL18Rα expression measured in NKTs 7 days after primary stimulation and 7 days after secondary stimulation in the same donor. Gray histograms represent isotype control (left). Summary data of IL18Rα expression from $n = 5$ donors. Mean is shown. ns, not significant; paired two-tailed *t* test (right). (C) Retroviral plasmids encoding GD2.CAR and iC9/cytokine constructs used in this study. LTR, long terminal repeat; scFv, single-chain variable fragment; H, hinge; TM, transmembrane domain; IL2SP, IL-2 signal peptide. (D) CAR and iC9/cytokine construct co-transduction strategy 6 days after isolation and primary stimulation, NKTs were transduced with iC9/cytokine encoding retroviruses, and 24 h later cells were harvested and transduced with GD2.CAR retroviral supernatant. (E) Two days after GD2.CAR transduction, co-transduced NKTs were stimulated using αGalCer-loaded aAPCs and expanded for 10 days. Transduction rate was then assessed by flow-cytometry analysis using antibodies specific to the GD2.CAR and Q8 marker. Representative flow-cytometry analysis of CAR/iC9 construct co-transduction efficiency 10 days after GD2.CAR transduction. (F) GFP-expressing CHLA255 ($GD2^{high}$, top) and CHLA136 ($GD2^{int}$, bottom) NB lines were co-cultured with CAR-NKTs co-transduced with the indicated constructs at different effector-to-target ratios. To determine tumor cytotoxicity, changes in GFP fluorescence were measured over the indicated period using the Incucyte system. Shown are results from a representative NKT donor of four with technical triplicates per condition. Mean (SD) is shown. ns, not significant; $^*p < 0.05$, $^{**}p < 0.01$, $^{***}p < 0.001$, $^{****}p < 0.0001$, one-way ANOVA.

Please cite this article in press as: Barragán Bravo et al., IL-18 metabolically reprograms CAR-expressing natural killer T cells and enhances their antitumor activity, Molecular Therapy (2026), https://doi.org/10.1016/j.ymthe.2026.01.001

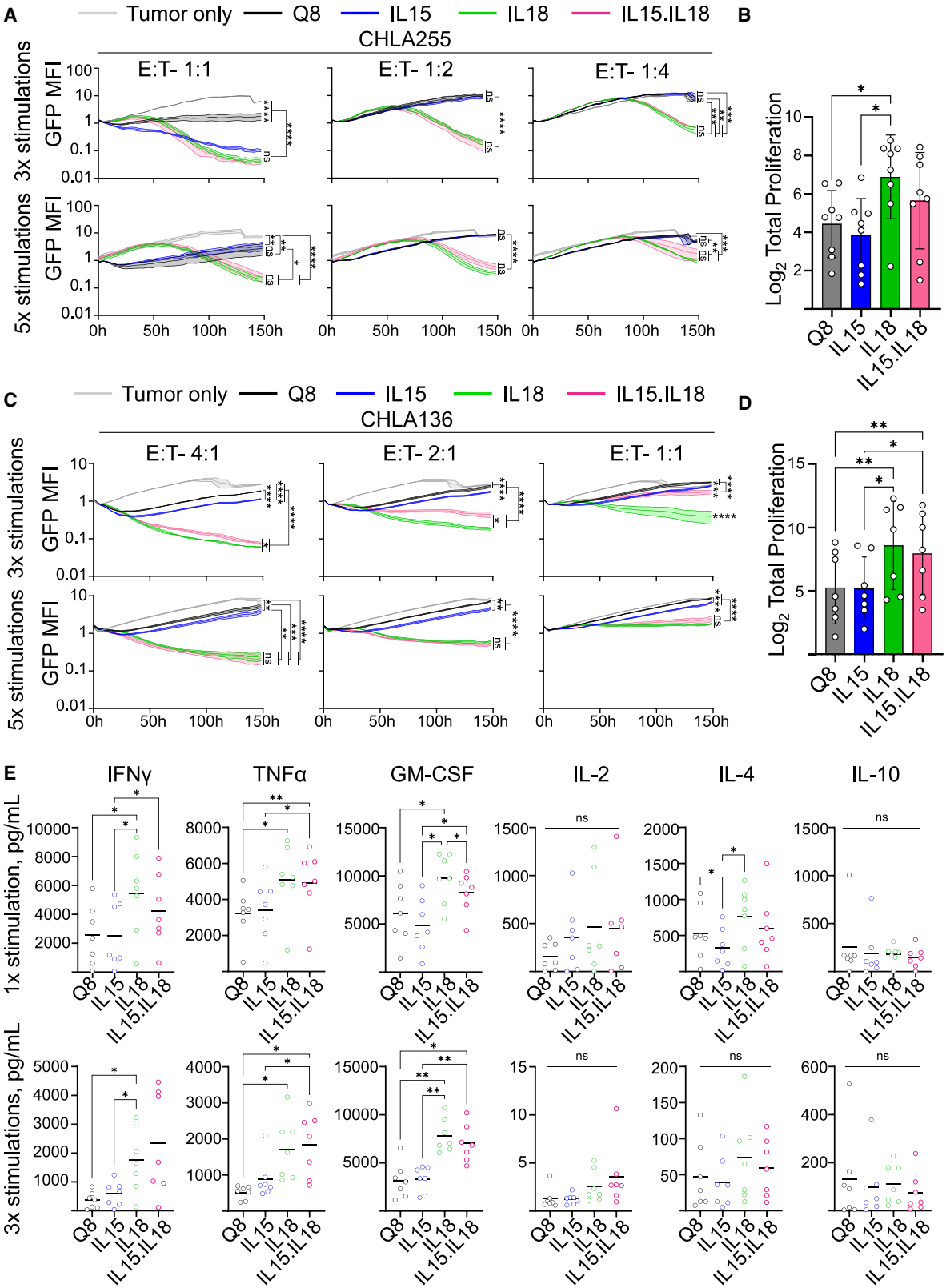

(legend on next page)

activated phenotype at baseline and does not have a notable impact on the expression of chemokine receptors involved in tumor trafficking.

Addition of the chemical inducer of dimerization (CID) rimiducid (AP1903) effectively eliminated $Q8^+$ cells, confirming the functionality of the iC9 safety switch (Figures S1H and S1I). Next, we characterized CAR-mediated *in vitro* cytotoxicity by co-culturing CAR-NKTs with CHLA255 ($GD2^{high}$) or CHLA136 ($GD2^{int}$) NB cell lines (Figure S1J). CAR-NKTs expressing iC9.IL18 and iC9.IL15.IL18 mediated significantly higher levels of cytotoxicity than iC9.Q8 and/or iC9.IL15 control cells at 1:2 and 1:4 effector-to-target (E/T) ratios in both cell lines (Figure 1F). This enhanced cytotoxic activity required continuous expression of IL-18 from the iC9.IL18 transgene as, unlike iC9.IL18 cells, CAR-NKTs exposed to soluble IL-18 during manufacturing did not mediate higher cytotoxicity levels or proliferate more than iC9.Q8 control cells (Figures S2A and S2B). These results show that NKTs maintain a high level of IL18Rα relative to other immune cells, with expression levels remaining unchanged between one and two stimulations, and that expressing IL-18 in GD2.CAR-NKTs increases activation marker expression and provides a greater boost to *in vitro* cytotoxicity against NB than IL-15.

IL-18 expression enhances CAR-NKT proliferation, antitumor activity, and cytokine secretion in a repeat tumor challenge assay

To determine how IL-18 and IL-15/IL-18 co-expression impacts GD2.CAR-NKT cytotoxicity after multiple encounters with tumor cells, we employed an *in vitro* repeat tumor challenge assay in which CAR-NKTs are serially stimulated with NB tumors every 3–4 days (Figure S3A). CAR-NKTs expressing iC9.IL18 and iC9.IL15.IL18 mediated significantly higher levels of cytotoxicity than iC9.Q8 and iC9.IL15 controls at multiple E/T ratios after three and five challenge cycles with CHLA255 and CHLA136 lines (Figures 2A and 2C). Additionally, CAR-NKTs expressing these constructs proliferated significantly more than controls, as measured after five challenge cycles and cumulatively over the course of the assay in a representative donor (Figures 2B, 2D, S3B, and S3C). Next, we stained for apoptosis marker annexin V after one, three, and five challenge cycles and did not detect significant differences among groups, suggesting that iC9.IL18 and iC9.IL15.IL18 do not increase GD2.CAR-NKT numbers by decreasing apoptosis rate (Figure S3D). Evaluating the cytokine secretion profile of GD2.CAR-NKTs after one and three challenge cycles revealed significant increases in IFN-γ, tumor necrosis factor α (TNF-α), and granulocyte macrophage colony-stimulating factor (GM-CSF) secretion from iC9.IL18 or iC9.IL15.IL18 transduced GD2.CAR-NKTs compared to iC9.Q8 and iC9.IL15 controls, while IL-2 and IL-10 were secreted at similar levels by all groups, and IL-4 showed variation between groups only after one round of stimulation (Figure 2E). The IFN-γ-to-IL-4 ratio was similar across groups after one stimulation but after three rounds, GD2.CAR-NKTs expressing iC9.IL15, iC9.IL18, and iC9.IL15.IL18 had significantly higher ratios than the iC9.Q8 control, suggesting a T helper 1 (Th1) skew in the former groups (Figure S3E). These results demonstrate that IL-18 co-expression alone and with IL-15 enhances GD2.CAR-NKT proliferation, cytotoxicity, and production of inflammatory cytokines more than IL-15 alone after serial tumor challenge. To determine whether IL-18 armoring can be used to enhance CAR-NKT function against other malignancies, we expressed iC9.IL18 in CAR-NKTs targeting glypican-3 (GPC3) and CD19 antigens and performed cytotoxicity and repeat tumor challenge assays using HUH7 and NALM6 cell lines, respectively. After manufacturing and after three tumor stimulations, GPC3.CAR-NKTs armored with IL-18 exhibited significantly greater cytotoxicity against HUH7 than IL-15 and Q8 controls (Figures S4A and S4B). iC9.IL18 expression also enhanced the proliferation of GPC3.CAR-NKTs after multiple stimulations with HUH7 cells (Figure S4C). CD19.CAR-NKTs (Figure S4D) armored with IL-18 mediated levels of cytotoxicity similar to those of controls after manufacturing and repeated tumor stimulations (Figures S4E and S4F), but IL-18 expression increased CD19.CAR-NKT proliferation in response to multiple challenges (Figure S4G). Taken together, these findings suggest that IL-18 boosts the functionality of NKTs expressing GD2, GPC3, or CD19.CARs.

IL18Rα expression is preserved in tumor-infiltrating CAR-NKTs

To investigate whether IL-18 signaling is likely to be functional in the solid TME, we asked whether tumor-infiltrating CAR-NKTs collected from a xenograft model of metastatic NB maintain IL18Rα expression. NSG mice were intravenously injected with CHLA255 NB cells followed 21 days later by CAR-NKTs, with tumor-free mice as controls (Figure S5A). This 3-week period between tumor cell and NKT infusion allows for the formation of liver metastases from which tumor-infiltrating CAR-NKTs can be isolated.

Figure 2. iC9.IL18 and iC9.IL15.IL18 enhance GD2.CAR-NKT *in vitro* antitumor cytotoxicity and proliferation after repeated tumor stimulation

(A) After three (top) and five (bottom) cycles of *in vitro* tumor stimulation, GD2.CAR-NKTs were rested overnight in fresh medium and co-cultured with CHLA255-GFP cells at the indicated E/T ratios. To determine tumor cytotoxicity, changes in GFP fluorescence were measured over the indicated period using the Incucyte system. Shown are results from one representative donor of four in two independent experiments with technical triplicates for each condition. Mean (SD) is shown. ns, not significant; $^*p < 0.05$, $^{**}p < 0.01$, $^{***}p < 0.001$, $^{****}p < 0.0001$, one-way ANOVA. (B) Summary of NKT proliferation for indicated groups after five rounds of stimulation with CHLA255 NB cells. Mean (SD), $n = 8$ donors in three independent experiments, $^*p < 0.05$, paired one-way ANOVA. (C) After three (top) and five (bottom) cycles of *in vitro* tumor stimulation, GD2.CAR-NKTs were rested overnight in fresh medium and co-cultured with CHLA136-GFP cells at the indicated E/T ratios. To determine tumor cytotoxicity, changes in GFP fluorescence were measured over the indicated period using the Incucyte system. Shown are results from one representative donor of four in two independent experiments with technical triplicates for each condition. Mean (SD) is shown. ns, not significant; $^*p < 0.05$, $^{**}p < 0.01$, $^{***}p < 0.001$, $^{****}p < 0.0001$, one-way ANOVA. (D) Summary of NKT proliferation for indicated groups after five rounds of tumor stimulation. Mean (SD), $n = 7$ donors in three independent experiments, $^*p < 0.05$, $^{**}p < 0.01$, paired one-way ANOVA. (E) Cytokine production after one (top) or three (bottom) stimulations with CHLA255 NB cells. Mean is shown; $n = 7$ donors in three independent experiments. ns, not significant; $^*p < 0.05$, $^{**}p < 0.01$, paired one-way ANOVA.

Please cite this article in press as: Barragán Bravo et al., IL-18 metabolically reprograms CAR-expressing natural killer T cells and enhances their antitumor activity, Molecular Therapy (2026), https://doi.org/10.1016/j.ymthe.2026.01.001

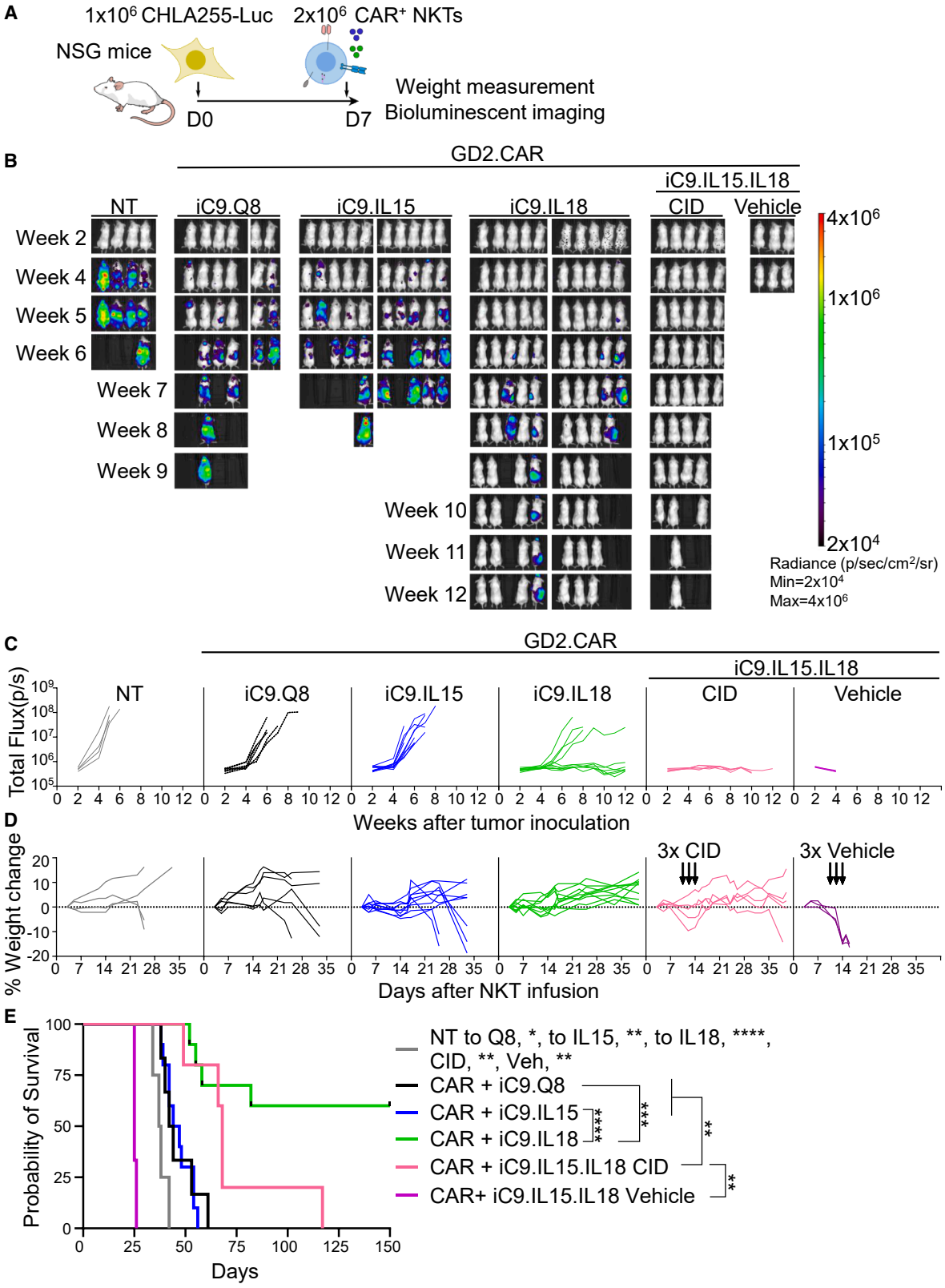

(legend on next page)

Three days after CAR-NKT infusion, mice were euthanized, and livers were harvested from both tumor-bearing and tumor-free animals for further processing and subsequent analysis by flow cytometry (Figures S5B and S5C). Compared to *ex vivo*-cultured CAR-NKTs from the same donor, tumor- and liver-infiltrating CAR-NKTs expressed lower levels of IL18Rα (Figure S5D). However, tumor-infiltrating NKTs expressed similar or higher levels of IL18Rα compared to cells collected from non-tumor-bearing mice (Figure S5E), suggesting that the IL-18 signaling pathway would remain functional in the TME.

IL-18 expression promotes superior GD2.CAR-NKT antitumor activity without toxicity

Next, we sought to determine whether IL-18 co-expression improves GD2.CAR-NKT antitumor activity in an *in vivo* xenogeneic mouse model of NB. NSG mice were intravenously injected with 1×10^6 firefly-luciferase-positive CHLA255 cells followed 7 days later with 2×10^6 GD2.CAR$^+$-NKTs co-transduced with iC9.IL18 or iC9.IL15.IL18, with iC9.Q8, iC9.IL15, and non-transduced NKTs as controls (Figure 3A). We found that both iC9.IL18 and iC9.IL15.IL18 increased the antitumor activity of GD2.CAR-NKTs compared to iC9.Q8- and iC9.IL15-treated groups based on tumor growth (Figures 3B and 3C). However, mice treated with iC9.IL15.IL18 cells experienced weight loss 12 days after CAR-NKT infusion and had to be treated with rimiducid (CID) or vehicle control, allowing for a built-in assessment of iC9 safety switch efficacy (Figure 3D). CID-treated mice rapidly regained weight, while those that received vehicle control continued to lose weight and had to be sacrificed. Flow-cytometry analyses revealed a significantly higher number of human CD45$^+$ (hCD45$^+$) cells in the spleens and peripheral blood of iC9.IL15.IL18 mice (treated with vehicle control) compared to iC9.Q8 mice (Figures S6A and S6B). In iC9.IL15.IL18 mice, CID treatment significantly reduced hCD45$^+$ and Q8$^+$ cell numbers compared to counts in vehicle control mice (Figures S6B and S6C). Mice treated with CID also showed lower levels of serum cytokines, including IL-15, IL-18, IFN-γ, TNF-α, mouse IL-6, and the chemokines macrophage inflammatory protein 1α (MIP-1α) and MIP-1β, compared to vehicle control mice, further indicating depletion of iC9-expressing cells (Figure S6D). In mice treated with iC9.IL18, we observed significantly increased serum levels of IL-18 and IFN-γ compared to iC9.Q8 or iC9.IL15 groups. Lastly, mice in the iC9.IL18- and CID-treated iC9.IL15.IL18 groups survived significantly longer than all others, although the vehicle-control-treated iC9.IL15.IL18 group did not survive as long as the control iC9.Q8 group ($p = 0.002$) (Figure 3E). To understand the mechanism behind the toxicities observed in iC9.IL15.IL18 mice, we sorted CAR$^+$-NKTs from the spleens of these mice when they presented with weight loss greater than 10% (Figures S6E and S6F). Compared to iC9.IL15.IL18 CAR-NKTs from the same donor after *in vitro* tumor stimulation, iC9.IL15.IL18 CAR-NKTs from treated mice showed 2,374 differentially expressed genes (DEGs) with an adjusted p value of <0.05 (Figure S6G). Specifically, mouse-isolated CAR-NKTs showed significant downregulation of *LEF1* and *CCR7*,[52] genes associated with a memory-like NKT phenotype, as well as upregulation of *CD86* and positive enrichment for a gene set enrichment analysis (GSEA) term related to activated immune cells (GO:0002323, normalized enrichment score = 1.84, and $p = 1.89 \times 10^{-4}$). We also observed upregulation of anti-apoptotic genes *BCL6*, *MCL1*, and *BCL11B*, suggesting that iC9.IL15.IL18 may drive the persistence of proliferative and activated CAR-NKTs.

In a separate experiment, we attempted to mitigate the toxicities associated with iC9.IL15.IL18 CAR-NKT infusion by decreasing the dose of administered CAR$^+$-NKTs. At the lowest dose levels (0.06×10^6 and 0.2×10^6 CAR$^+$-NKTs), the NKTs mediated little to no control of CHLA255 NB tumors compared to non-transduced NKTs, and no survival benefit was observed (Figures S7A and S7B). At the 0.6×10^6 CAR$^+$-NKT dose level, mice exhibited comparable antitumor activity and survival probability to mice treated with 2×10^6 iC9.IL18 NKTs, but mice in the iC9.IL15.IL18 group still experienced weight loss (Figures S7C and S7D). These findings indicate that a lower dose of iC9.IL15.IL18 CAR-NKTs can still lead to lethal toxicities in mice, limiting the translational potential of this cytokine combination. Based on these results, we excluded the iC9.IL15.IL18 construct from further testing and focused on evaluating iC9.IL18.

Given that GD2 expression levels can be heterogeneous in many NB tumors,[53] we evaluated the *in vivo* antitumor activity of iC9.IL18 GD2.CAR-NKTs in a second mouse model of NB based on CHLA136 NB cells, which express intermediate levels of GD2 (Figures S8A and S1J). Mice treated with iC9.IL18 cells had lower tumor bioluminescence signal than iC9.Q8-and iC9.IL15 mice over 7 experimental weeks and did not experience weight loss (Figures S8B–S8D). As in the CHLA255 model, mice treated with iC9.IL18 cells survived significantly longer than those in all other groups (Figure S8E). Thus, our results show that IL-18 safely enhances GD2.CAR-NKT antitumor activity more than IL-15 in two *in vivo* NB mouse models with different levels of GD2 expression.

Since iC9.IL18 expression boosted CAR-NKT proliferation after repeat tumor challenge *in vitro*, we proceeded to evaluate CAR-NKT proliferation *in vivo* by co-transducing GD2.CAR-NKTs expressing iC9.cytokine constructs with a firefly luciferase (FFLUC)

Figure 3. iC9.IL18 endows CAR-NKTs with superior antitumor activity in a mouse xenograft model of NB without toxicities

(A) NSG mice were injected via tail vein with luciferase-expressing CHLA255 NB cells, and CAR-NKTs were infused through the same route 7 days later. Tumor growth was assessed weekly by bioluminescence imaging. Weight was measured every other day. (B) CHLA255 tumor progression was measured by bioluminescence imaging after administration of the indicated CAR-NKTs (n = 3–10 mice per group). (C) Quantification of bioluminescence signal in (B). (D) Percent weight change for mice in (B) after NKT infusion. Timing of CID/vehicle control administration is indicated by arrows. (E) Kaplan-Meier survival curve for mice in (B). *$p < 0.05$, **$p < 0.01$, ***$p < 0.001$, ****$p < 0.0001$, log rank (Mantel-Cox). Shown are results from one of two independent experiments.

retroviral construct. NSG mice were infused with CHLA255 NB tumors followed 7 days later by FFLUC$^+$ iC9/CAR-NKTs (Figure S9A). Bioluminescent signal was measured at baseline and every other day after CAR-NKT infusion (Figure S9B). Mice treated with iC9.IL18 GD2.CAR-NKTs exhibited significantly higher bioluminescent signal over time than mice that received iC9.Q8 or iC9.IL15 cells (Figure S9C), demonstrating that iC9.IL18 drives greater CAR-NKT proliferation *in vivo*.

We also performed an experiment to determine whether IL-18 expression impacts the *in vivo* infiltration profile of CAR-NKTs using the same xenograft model of metastatic NB and experimental design employed to assess IL18Rα expression in tumor-infiltrating CAR-NKTs (Figure S5A). Twenty-one days after CHLA255 injection, mice were treated with iC9.Q8, iC9.IL15, or iC9.IL18 NKTs, and organs were harvested 3 days later. Flow-cytometry analysis of spleens (Figure S10A) and bone marrow (Figure S10B) from these mice showed no significant differences in the percentage of hCD45$^+$ cells present in these organs among groups, but lungs from iC9.IL18-treated mice had a significantly lower percentage of hCD45$^+$ cells compared to lungs from Q8 and IL-15 mice (Figure S10C). To accurately assess GD2.CAR-NKT infiltration at tumor sites, we performed immunohistochemistry (IHC) for human tyrosine hydroxylase (hTH), a diagnostic marker for NB tumors,[54] and human CD3 in tissue sections collected from mouse livers. Positive hTH staining was observed in tissue sections from all groups (Figure S10D). Quantification of intra- and peritumoral hCD3$^+$ cells in these tissue sections revealed no significant differences in cell number among groups (Figures S10E and S10F). These findings suggest that shortly after infusion, IL-18 does not affect CAR-NKT infiltration to the spleen, bone marrow, or tumor sites in the liver but significantly decreases CAR-NKT presence in the lungs of treated mice.

Although we did not observe weight loss in iC9.IL18-treated mice, we still performed a detailed pathological examination of mouse tissues 2 weeks after CAR-NKT infusion to assess for toxicity. Small and large intestine, esophagus, stomach, and skin samples demonstrated no signs of pathological abnormalities in any of the tested groups (Figure S11A). Lung sections from all groups showed signs of vascular congestion in alveoli, and all groups showed signs of focal diffuse autolysis in the kidney. Importantly, brain sections of iC9.IL18-treated mice did not show abnormal pathology (Figure S11B). Taken together, these findings show that IL-18 expression enhances the antitumor activity and proliferation of CAR-NKTs in xenograft models of metastatic NB without negatively affecting their safety profile and with minor impacts on tissue-infiltration sites.

IL-18 expression drives transcription of activation-related, mitochondrial, and metabolic genes in CAR-NKTs

To determine how IL-18 impacts molecular pathways in GD2.CAR-NKTs, we performed bulk RNA sequencing (RNA-seq) of samples at baseline and after one or three stimulations with CHLA255 NB cells, using IL-15-expressing CAR-NKTs as control (Figure S12A). A comparison of IL-18- versus IL-15-expressing CAR-NKTs revealed 2,751 DEGs at baseline, 2,009 after one tumor stimulation, and 1,165 after three stimulations, with an adjusted p value of <0.05 (Figures S12B–S12D). At baseline and after one tumor stimulation, we observed significant downregulation of *TCF7* in IL-18-expressing cells compared to IL-15, suggesting an early transition from a memory-like state toward an effector state (Figures 4A–4C). Accordingly, we also observed downregulation of *IL7R* and *CD27*, which we have previously reported to be upregulated in memory-like NKTs,[51,52] in the IL-18 group after one tumor stimulation. At baseline, IL-18 expressing CAR-NKTs showed increased expression of genes associated with effector differentiation including *BATF3*, *BATF*, *CD38*, and *IFNG*, and at all three time points, significant upregulation of activation-related genes including *IL-2RA* (CD25) and *CD86* was observed (confirmed by flow cytometry at baseline, Figure S12E). In support of these observations, GSEA revealed significant enrichment of activation- and cytokine-related terms in IL-18- versus IL-15-expressing CAR-NKTs (Figure 4D). Mitochondrial- and metabolism-related terms were also significantly enriched in the IL-18 group at all time points, and we detected signatures of MYC targets and mTOR signaling, known regulators of lymphocyte metabolism (Figures 4E and S12F).[55,56] These findings suggest that the transcriptional program driven by IL-18 in CAR-NKTs is distinct from that of IL-15, and that many of the changes associated with IL-18 expression are related to increases in CAR-NKT mitochondrial and metabolic activity at baseline and after tumor stimulation.

Single-cell RNA-seq identifies IL-18-specific gene clusters

We performed single-cell transcriptomic analyses (single-cell RNA-seq [scRNA-seq]) to define the effects of IL-18 expression on CAR-NKT transcription at single-cell resolution. Using tumor-stimulated iC9.IL15 and iC9.IL18 CAR-NKTs from three healthy donors (Figure S12A), we captured a total of 21,436 cells, 58.35% of which aligned to the GD2.CAR sequence. Unsupervised single-cell clustering analysis revealed the presence of eight unique expression clusters in CAR$^+$ NKTs; IL-15-expressing CAR-NKTs were over-represented in cluster 3, while IL-18-expressing cells were over-represented in clusters 0, 2, and 4 (Figures 5A, 5B, and S13). Genes upregulated in the IL-15 cluster included *DUSP2*, *BAX*, and *CISH*, a negative regulator of IL-15 signaling,[57,58] while IL-18 clusters included *SOX4* and *MYC* (Figure 5C). Next, cell-cycle analysis demonstrated that cells in S phase overlapped with IL-18 clusters, consistent with the increased proliferation observed in these cells after repeated *in vitro* tumor stimulation (Figure 5D). Importantly, we found that cells in IL-18-related clusters had lower expression of exhaustion gene signatures than cells in the IL-15 cluster, consistent with the observation that IL-18 drives antitumor activity, proliferation, and cytokine secretion after multiple rounds of *in vitro* tumor challenge (Figure 5E).

IL-18 expression promotes oxidative phosphorylation and glycolysis in CAR-NKTs

Since our transcriptomic analyses showed enrichment of mitochondria- and metabolism-related GSEA terms in the IL-18 group, we performed several metabolic tests to further explore these findings.

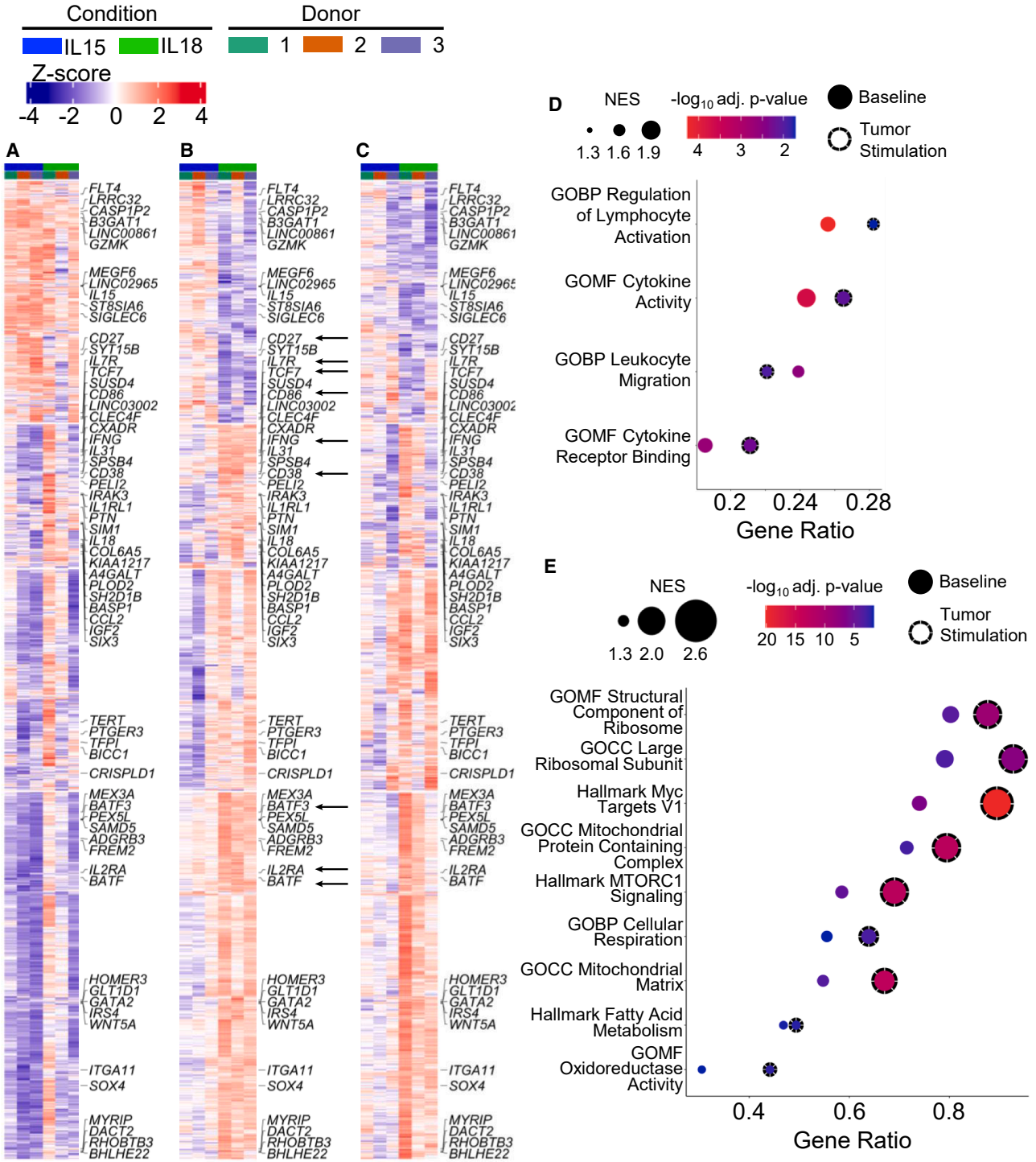

Figure 4. IL-18 expression drives transcription of activation-related, mitochondrial, and metabolic genes in CAR-NKTs

Gene expression heatmaps generated from CAR-NKTs expressing iC9.IL18 or iC9.IL15 at baseline (A) and after one (B) or three (C) tumor stimulations. Heatmaps were generated from *k*-means clustering of differentially expressed genes with $p < 0.05$ after one tumor stimulation. Arrows indicate genes highlighted in the body of the text. (D) GSEA terms significantly enriched in iC9.IL18 versus iC9.IL15 CAR-NKTs at baseline (no border) and after one tumor stimulation (border). (E) GSEA metabolism-related terms significantly enriched in iC9.IL18 versus iC9.IL15 CAR-NKTs at baseline (no border) and after one tumor stimulation (dashed border).

Please cite this article in press as: Barragán Bravo et al., IL-18 metabolically reprograms CAR-expressing natural killer T cells and enhances their antitumor activity, Molecular Therapy (2026), https://doi.org/10.1016/j.ymthe.2026.01.001

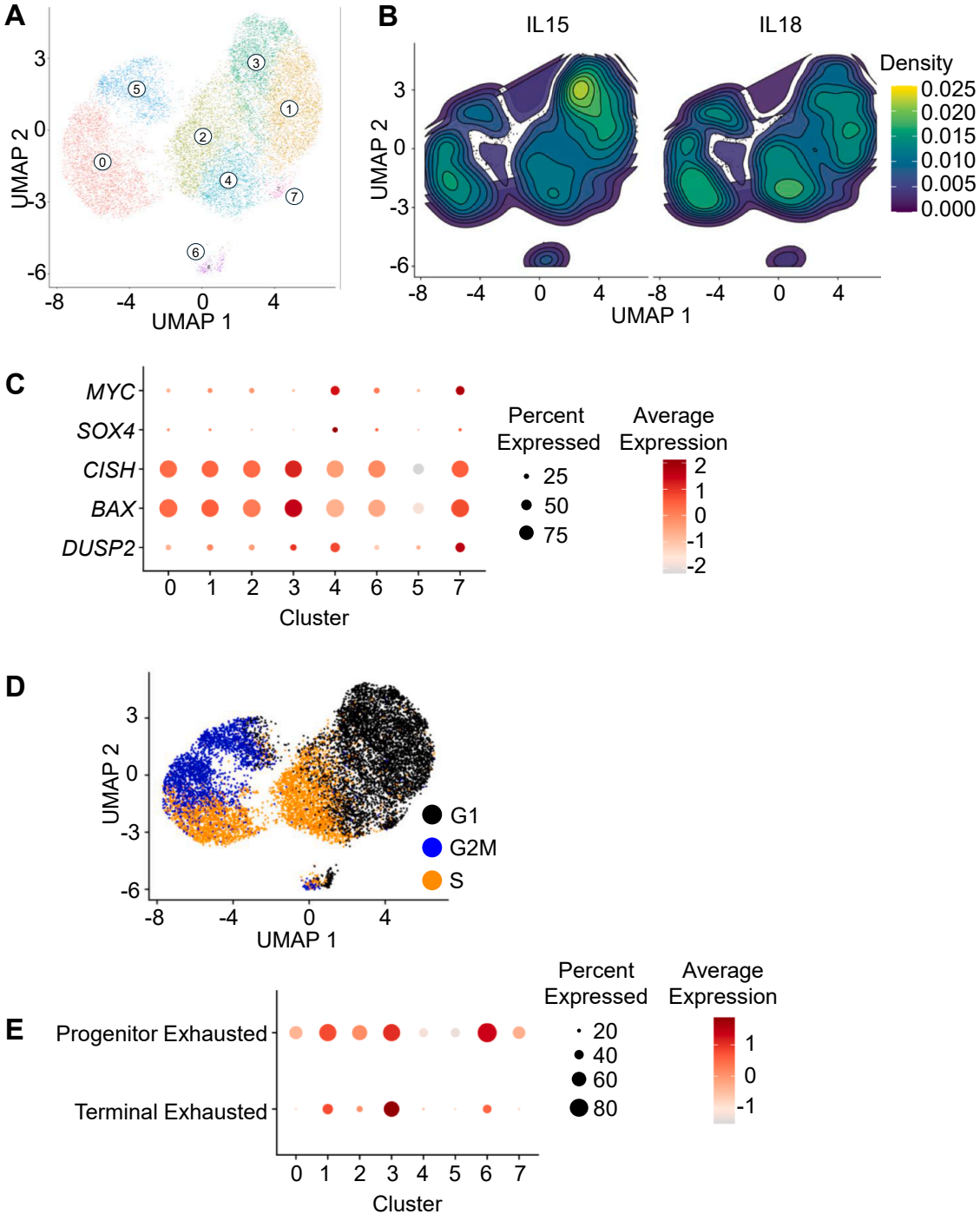

Figure 5. Single-cell gene-expression analyses identify IL-18- and IL-15-specific gene clusters

(A) Uniform manifold approximation and projection analysis of integrated iC9.IL15 and iC9.IL18 CAR-NKTs after one tumor stimulation. (B) Integrated data displaying density of iC9.IL15 and iC9.IL18 expressing CAR-NKTs. (C) Dotplot depicting differences in percentage and average expression for indicated genes in clusters 0–7. (D) Cell-cycle analysis of single-cell RNA-sequencing data in (A). (E) Progenitor and terminal exhaustion gene signature percentage and average expression for clusters 0–7.

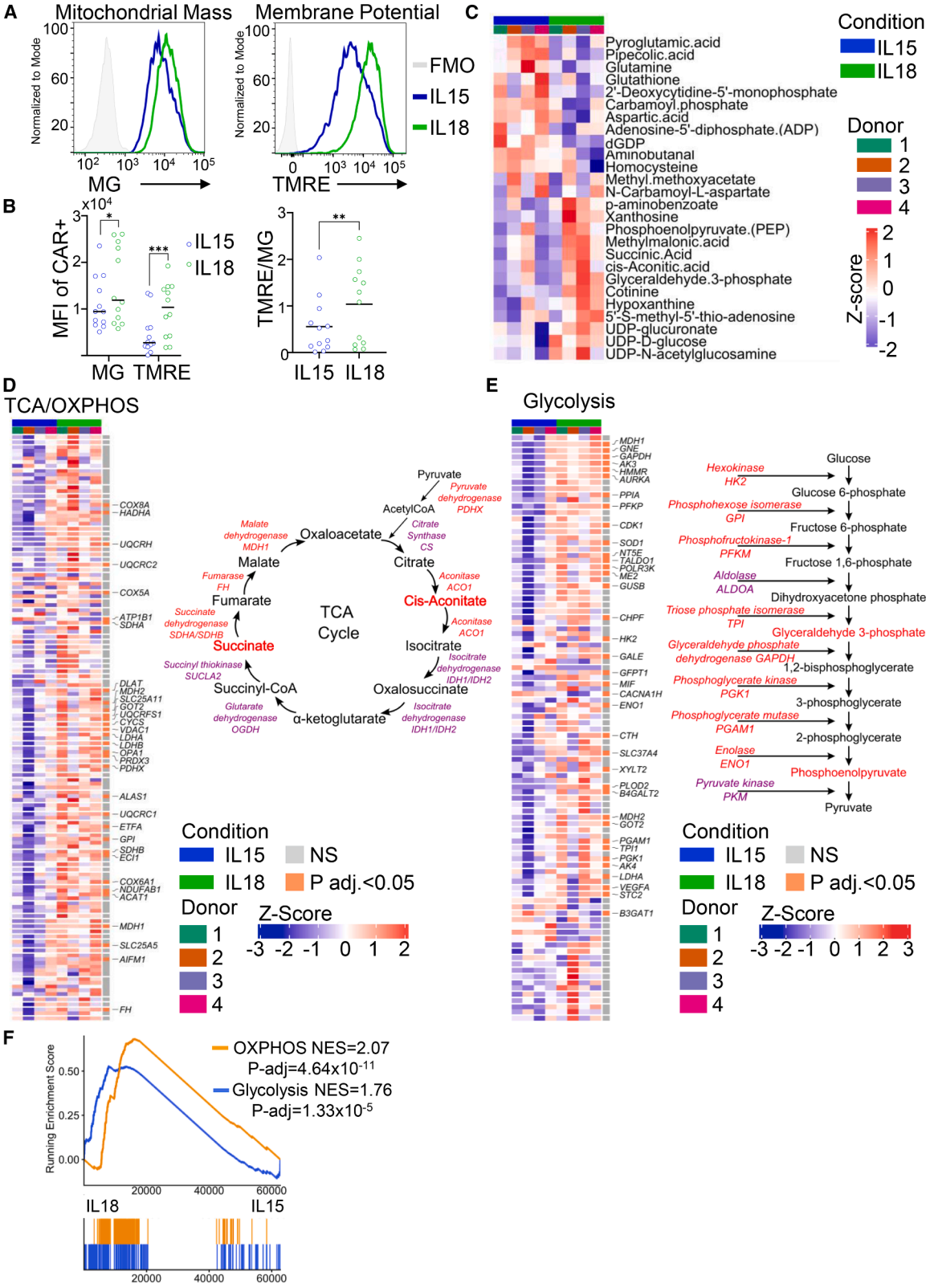

(legend on next page)

Please cite this article in press as: Barragán Bravo et al., IL-18 metabolically reprograms CAR-expressing natural killer T cells and enhances their antitumor activity, Molecular Therapy (2026), https://doi.org/10.1016/j.ymthe.2026.01.001

First, we assessed mitochondrial fitness, a key predictor of T cell function,[59] by measuring mitochondrial mass (MitoTracker green [MG]) and membrane potential (tetramethylrhodamine ethyl ester perchlorate [TMRE]) in CAR-NKTs before and after tumor stimulation. Both measures were significantly greater in CAR-NKTs expressing iC9.IL18 versus iC9.IL15 at both time points, and the TMRE/MG ratio was also significantly greater in iC9.IL18 CAR-NKTs, reflecting increased activity per mitochondrion (Figures S14A, S14B, 6A, and 6B).[60] Given that the fatty acid metabolism term was also significantly enriched in iC9.IL18 expressing CAR-NKTs, we measured fatty acid uptake before and after tumor stimulation and found that iC9.IL18 CAR-NKTs had a significantly higher level of BODIPY uptake than iC9.IL15 cells at both time points (Figure S14C). Additional targeted metabolomics analyses identified 17 differentially expressed metabolites (DEMs) in unstimulated CAR-NKTs expressing iC9.IL18 versus iC9.IL15 ($p < 0.05$), which increased to 21 after stimulation (Figures S14D and 6C). Stimulated CAR-NKTs expressing IL-18 showed significant enrichment of tricarboxylic acid (TCA)-cycle metabolites succinate and *cis*-aconitate as well as increased levels of genes encoding TCA-cycle enzymes *SDHB*, *MDH2*, *MDH1*, *FH*, and *SDHA*, indicating increased TCA-cycle activity (Figure 6D). The glycolytic pathway also appeared to be more active in stimulated CAR-NKTs expressing IL-18 versus IL-15 based on higher levels of glycolytic intermediates phosphoenolpyruvate and glyceraldehyde 3-phosphate, significant upregulation of genes encoding glycolytic enzymes (*HK2*, *GPI*, *PFKM*, *TPI1*, *GAPDH*, *PGK1*, *PGAM1*, *ENO1*, and *DLAT*), and higher levels of glucose uptake (Figures 6E and S14E). These transcriptomic changes resulted in significant enrichment of oxidative phosphorylation and glycolysis gene signatures in IL-18-expressing CAR-NKTs before stimulation (Figure S14F) and after stimulation (Figure 6F); expression of these gene signatures was concentrated in the IL-18-associated clusters (0, 2, and 4) identified in our scRNA-seq analyses versus the IL-15-associated cluster (3) (Figure S14G). Next, we performed Seahorse assays to assess the functional relevance of these gene-expression changes. iC9.IL18 CAR-NKTs showed a trend toward increased basal and maximal respiration compared to iC9.IL15 (Figure S14H), and we also observed similar trends in glycolytic capacity and reserve in iC9.IL18- versus iC9.IL15-expressing CAR-NKTs (Figure S14I).

To identify other metabolic pathways that are impacted by IL-18 expression, we performed pathway enrichment analysis using the DEMs we identified above and found that the "glutamate metabolism" term was significantly enriched in iC9.IL18 CAR-NKTs before and after stimulation (Figures S15A and S15B). Indeed, glutamine was the most downregulated metabolite in iC9.IL18 CAR-NKTs in both conditions (Figure S15C) despite increased expression of glutamine transporters *SLC7A5* and *SLC1A5* (Figure S15D). We also noted differential expression of transcripts related to glutamine metabolism, including *GLUL*, *PPAT*, *GFPT1*, *CAD*, *GPT2*, and *GOT2*. These findings indicate activation of the glutaminolysis pathway and are consistent with the role of this amino acid in T cell activation, proliferation, and cytokine production.[55,61] The "purine metabolism" term was also significantly enriched in iC9.IL18 CAR-NKTs, as evidenced by differential expression of inosine, hypoxanthine, L-aspartic acid, xanthosine, glutamine, deoxyguanosine diphosphate, and adenosine diphosphate either before stimulation (Figure S14D) or after stimulation (Figure 6C). Notably, inosine, which has been associated with promoting T cell fitness,[62,63] was upregulated in iC9.IL18 CAR-NKTs before stimulation. Hypoxanthine, a by-product of inosine metabolism, was significantly upregulated after stimulation, suggesting that this pathway remains active in both conditions. Transcriptomic analyses supported the involvement of this pathway by revealing significant increases in the level of expression for several genes involved in purine metabolism in IL-18-expressing CAR-NKTs before and after stimulation (Figure S15E). Enrichment of the purine metabolism pathway is consistent with the requirement for an increase in the nucleotide pool after T cell activation.[64,65]

Overall, our findings demonstrate that IL-18 expression has broad effects on CAR-NKT metabolism, including promoting oxidative phosphorylation and glycolysis, providing a mechanistic explanation for the observed increase of CAR-NKT functional fitness and antitumor activity in NB models.

DISCUSSION

Solid tumors remain largely resistant to therapeutic immune cell products such as CAR-redirected T, NK, and NKTs due in part to the highly suppressive TME. A promising strategy for overcoming TME-mediated suppression is to engineer antitumor effector cells to express stimulatory cytokines.[30,32,66] Given that cytokine receptor expression levels vary among different lymphocyte subsets and can also depend on differentiation stage and activation status,[48,67,68] it is crucial to design cell-type-specific studies for evaluating candidate

Figure 6. IL-18 expression broadly reprograms CAR-NKT metabolism

(A) Flow-cytometry histograms depicting MitoTracker green (MG, left) and tetramethylrhodamine ethyl ester perchlorate (TMRE, right) staining in CAR$^+$-NKTs from a representative donor 3 days after tumor stimulation. (B) Summary data for MG and TMRE staining after tumor stimulation (left; mean, $n = 12$ donors, three independent experiments) and TMRE-to-MG ratio calculated from values in left panel (right; mean, $n = 12$ donors, three independent experiments). $^*p < 0.05$, $^{**}p < 0.01$, $^{****}p < 0.0001$, paired two-tailed *t* test. (C) Differentially expressed metabolites in iC9.IL18 versus iC9.IL15 expressing CAR-NKTs 24 h after stimulation with plate-bound 1A7 antibody ($n = 4$ donors, $p < 0.05$). (D) Heatmap depicting oxidative phosphorylation metabolite-related genes in CAR-NKTs after one stimulation (left). TCA-cycle schematic showing significantly upregulated molecules in red text. Purple italic text indicates upregulated transcripts with $p < 0.05$ and adjusted $p > 0.05$ (right). (E) Heatmap depicting glycolysis metabolite-related genes in CAR-NKTs after one stimulation (left). Glycolysis pathway schematic showing significantly upregulated molecules in red text. Purple italic text indicates upregulated transcripts with $p < 0.05$ and adjusted $p > 0.05$ (right). (F) GSEA of oxidative phosphorylation (yellow) and glycolysis signatures (blue) in stimulated CAR-NKTs expressing iC9.IL18 versus iC9.IL15.

cytokines that take these factors into consideration. In this study, we explored for the first time how IL-18 impacts CAR-NKT functionality, antitumor activity, and toxicity in preclinical NB models. Compared to IL-15, the only cytokine that has so far been evaluated clinically in therapeutic CAR-NKTs,[66] IL-18 enhanced CAR-NKT effector function and antitumor activity in NB models while maintaining a favorable safety profile.

Surprisingly, we discovered that human NKTs expressed significantly higher levels of IL18Rα than NK and conventional T cells and that IL18Rα expression is maintained in tumor-infiltrating CAR-NKTs relative to normal tissues, suggesting that IL-18 signaling is particularly relevant for this cell type. In both short-term cytotoxicity and serial tumor challenge assays, CAR-NKTs expressing iC9.IL18 and iC9.IL15.IL18 mediated higher levels of cytotoxicity against both $GD2^{high}$ and $GD2^{int}$ NB cells than iC9.Q8 and iC9.IL15 control cells. Cytotoxicity against $GD2^{int}$ cells is of particular clinical relevance, as GD2 expression is variable in NB patients, and lower GD2 expression has been observed as an escape mechanism in NB patients treated with GD2-specific monoclonal antibodies,[69] potentially playing a role in resistance to GD2.CAR-redirected immunotherapy. Additionally, IL-18 expression increased the functionality of both GPC3.CAR and CD19.CAR-NKTs, suggesting that IL-18-armored CAR-NKTs can have therapeutic applications beyond NB.

Consistent with these observations, IL-18-containing constructs also promoted robust CAR-NKT proliferation and induction of multiple cytokine responses following *in vitro* serial tumor challenge compared to iC9.Q8 or iC9.IL15. *In vivo*, IL-18-expressing CAR-NKT groups mediated superior tumor clearance compared to controls, but mice treated with iC9.IL15.IL18 experienced toxicities including weight loss, increased systemic expansion of CAR-NKTs, and elevated serum concentrations of human cytokines. Gene-expression analysis of iC9.IL15.IL18 CAR-NKTs sorted from mice with evidence of toxicity revealed that these cells displayed an activated effector phenotype and showed upregulation of anti-apoptotic genes compared to cells stimulated *in vitro*, demonstrating the emergence of a unique transcriptional program resulting from the combination of IL-15 and IL-18 *in vivo*. Synergy between IL-15 and IL-18 has previously been reported in NK cells, and the NKT hyperactivation that we observed is therefore not without precedent.[70,71] A lower dose of iC9.IL15.IL18 CAR-NKTs was not sufficient to avoid toxicity-associated weight loss in treated mice; therefore, taking advantage of IL-15/IL-18 synergism would require the application of novel cell-engineering strategies[72,73] outside the scope of the present work. Hence, we excluded the IL-15/IL-18 combination from further consideration as a clinical candidate, focusing instead on iC9.IL18, which mediated potent antitumor activity in $GD2^{high}$ and $GD2^{int}$ NB models. CAR-NKTs expressing iC9.IL18 proliferated and persisted significantly more *in vivo* than iC9.Q8 and iC9.IL15 controls, consistent with their increased proliferation in an *in vitro* repeat tumor challenge assay. Importantly, iC9.IL18 treatment did not cause toxicity in mice, as revealed by a detailed pathological examination. These findings align with recent clinical data demonstrating that IL-18-expressing CD19.CAR-T cells are safe in lymphoma patients,[42,74] reinforcing the feasibility of incorporating IL-18 into CAR-based immunotherapies. Moreover, analysis of liver tumor sites showed that IL-18 expression did not alter the infiltration profile of GD2.CAR-NKTs, suggesting that the *in vivo* benefits of IL-18 armoring are not due to increased tumor infiltration of these cells but, rather, enhanced proliferation and cytotoxic function.

Although CAR-NKTs expressing iC9.IL18 did not generate toxicity in mice, incorporating the iC9 safety switch into the final clinical construct is critical to ensuring that the therapeutic cells can be eliminated after infusion if needed. iC9 has been validated in cell therapy trials as an effective safety switch, including a recent report in GPC3-positive solid-tumor patients treated with GPC3.CAR-T cells co-transduced with an iC9.IL-15 construct.[66] This study also demonstrated the advantage of a system where the CAR is encoded by one construct and the iC9 switch and cytokine by a second construct; elimination of IL-15-producing cells by iC9 activation effectively controlled toxicity while providing evidence of objective tumor control.[66] Our results also validated the functionality and robustness of the iC9 switch, which was activated successfully following CID treatment *in vitro* and *in vivo* in mice receiving iC9.IL15.IL18 CAR-NKTs.

Importantly, bulk transcriptomics, scRNA-seq, and metabolomic profiling revealed that IL-18 induces a distinct transcriptional and metabolic program in CAR-NKTs. Compared to IL-15, IL-18 expression increased mitochondrial activity, oxidative phosphorylation, glycolysis, and glutaminolysis. These processes have been previously been linked with T cell activation[75,76] and are likely to be important for sustained effector function of CAR-redirected immune cells at tumor sites. Indeed, the ability of IL-18 expressing CAR-NKTs to exploit different metabolic pathways and nutrients could prove advantageous for persistence in the nutrient-poor TME, and evaluating the roles of specific metabolites in CAR-NKT function would provide a focus for future studies. IL-18-armored CAR-T cells have also been shown to remodel the TME, including increasing numbers of endogenous NK cells, dendritic cells, and CD8 T cells[18] at tumor sites and decreasing the proportion of tumor-resident M2 macrophages and regulatory T cells in immunocompetent mouse models.[37,38] A recent report on IL-18-armored CD371.CAR-T cells in acute myeloid leukemia patients demonstrated an upregulation of activation markers and IL-18 response signature in endogenous NK cells,[43] providing further validation for the immunostimulatory effects of IL-18 in the clinical setting. Collectively, this information suggests that transgenic IL-18 expression in CAR-NKTs will promote remodeling of the TME and likely enhance the intrinsic antitumor properties of CAR-NKTs in immunocompetent hosts.

In conclusion, our findings demonstrate that IL-18 enhances the antitumor efficacy of CAR-NKTs by promoting metabolic fitness and effector function without increasing off-target toxicity. These results support the clinical translation of IL-18-expressing CAR-NKTs

for the treatment of NB and, potentially, other tumor types. Future studies should focus on optimizing IL-18-based CAR-NKT therapies to maximize their therapeutic potential while minimizing toxicity, paving the way for more effective and durable cancer immunotherapies.

MATERIALS AND METHODS

Cell lines

CHLA255 and CHLA136 NB cell lines were cultured in IMDM medium supplemented with 20% fetal bovine serum (FBS) and GlutaMAX (Gibco, 35050061). HEK293T cells were maintained in IMDM supplemented with 10% FBS and GlutaMAX. The HUH7 hepatocellular carcinoma (HCC) cell line was cultured in low-glucose DMEM supplemented with 10% FBS and GlutaMAX. Luciferase-transduced or GFP-transduced CHLA255 or CHLA136 cell lines were used in indicated experiments. K562 artificial antigen-presenting cells (aAPCs)[51] and NALM6-GFP cells were maintained in RPMI-1640 supplemented with 10% FBS and GlutaMAX. All cell lines were routinely tested for *Mycoplasma* contamination. Cell line identities were validated at MD Anderson Cancer Center (Houston, TX) using the short tandem repeat method within 1 year of use.

Plasmids

The GD2.28ζ, FFLUC-GFP, and GPC3.28.BBζ plasmids have been previously described.[77–79] The retroviral CD19.CAR construct used in this study encoded the FMC63 scFv, CD8α transmembrane domain, CD28 co-stimulatory domain, and a CD3ζ signaling domain. iC9, cytokines, and Q8 sequences were cloned into the SFG gamma-retroviral backbone[80] using NEBuilder HiFi DNA Assembly master mix (NEB, E2621L). The IL-2-SP-IL-18 sequence was synthesized by IDT. iC9,[81] IL-15,[31] and Q8[47] sequences were PCR-amplified from existing constructs using Platinum SuperFi II PCR master mix (Thermo Fisher, 12368010). The pNFKB reporter construct was generated by PCR amplifying from the NFKB-eGFP from pSIRV-NF-κB-eGFP construct (Addgene, 118093) (a gift from Peter Steinberger)[82] and inserting the fragment into a lentiviral backbone by HiFi DNA assembly, followed by an SFFV promoter and the tEGFR transduction marker. The psPAX2 and pMD2.G plasmids (Addgene, 12260 and 12259, respectively) were gifts from Didier Trono.

Virus production

Retroviral particles were generated as previously described,[83] as were lentiviral particles.[84]

NKT manufacturing and transduction

NKTs were isolated from the buffy coats of healthy human donors (Gulf Coast Regional Blood Center) and expanded as previously described.[48] Six days after isolation, NKTs were retrovirally transduced with iC9/cytokine constructs, and on the following day, iC9-NKTs were collected and transduced with the CAR construct. In some experiments, NKTs were also transduced with FFLUC_GFP retrovirus on day 6, followed by iC9.cytokine retrovirus on day 7 and CAR retrovirus on day 8. For pNFKB reporter construct experiments, equal volumes of CAR (retroviral) and reporter (lentiviral) supernatants were mixed and spun down at 4,000 × *g* for 1.5 h at 32°C onto retronectin-coated non-tissue-culture-treated 24-well plates. Two days after the second transduction, NKTs were transferred to 24-well G-Rex plates and stimulated with irradiated K562 aAPCs[51] in the presence of 100 ng/mL α-galactosylceramide (αGalCer; Avanti Polar Lipids, 86700P-1mg) and 200 U/mL IL-2 (National Cancer Institute/TECIN, 23-6019). NKTs were expanded for an additional 10–12 days and then used immediately or cryopreserved for subsequent experiments.

In vitro cytotoxicity assays: Incucyte system

In vitro cytotoxicity of NKTs co-transduced with the CAR and IL-18 and/or IL-15 was evaluated using an Incucyte S3 imaging system. One day before starting the assay, 1×10^4 GFP-expressing NB or HCC cells were plated in each well of a flat-bottom tissue-culture-treated 96-well plate and incubated for 5 min at room temperature to allow for even distribution of cells on the bottom of the wells. On the same day, CAR-transduced and non-transduced NKTs were thawed and recovered overnight in medium containing 200 U/mL of IL-2. On the next day, NKTs were washed and resuspended in fresh medium without cytokines. NKTs were serially diluted to achieve the indicated E/T ratios and added to the tumor cells plated the day before. Incucyte imaging was performed every 4 h. Images were analyzed using Incucyte software (Sartorius).

Repeat tumor stimulation assay

Cryopreserved NKTs were thawed and rested overnight in the presence of 200 U/mL IL-2. On the following day, cells were washed and resuspended in fresh medium containing 50 U/mL IL-2, and 3×10^6 CAR^+-NKTs were plated with an equal number of tumor cells per well of a 24-well G-Rex. Total live CAR^+-NKT cell and tumor cell numbers were determined every 3–4 days (CHLA255 model and NALM6 model) or 4–5 days (CHLA136 model) by flow cytometry using CountBright Plus counting beads (Thermo Fisher, C36995). After counting, 3×10^6 CAR^+-NKTs were replated with an equal number of tumor cells for a total of five tumor stimulation rounds. For the repeat stimulation assay with HUH7 cells and GPC3.CAR-NKTs, 0.1×10^6 HUH7-GFP cells were plated per well of a 48-well plate in a final volume of 300 μL of NKT medium. On the following day, 0.2×10^6 GPC3.CAR^+-NKTs (E/T = 2:1) were plated into appropriate wells in 600 μL of NKT medium, each well was supplemented with IL-2 at a final concentration of 50 U/mL, and tumor killing was determined by imaging in the Incucyte system. Every 4 days, cells were counted using an automated cell counter, CAR percentage was determined separately by flow cytometry staining, and 0.2×10^6 CAR^+-NKTs were then replated with fresh HUH7-GFP cells. After three or five tumor stimulations, NKTs were rested overnight in fresh medium containing 200 U/mL IL-2 for *in vitro* cytotoxicity testing at different ratios with respective cell lines or for RNA isolation. NKTs were rested for 2 additional days for flow-cytometry phenotyping. Evaluation of cytotoxicity after repeat tumor stimulation was performed as described in "*in vitro* cytotoxicity assays: Incucyte system."

Luminex assays

NKTs were washed and resuspended in fresh medium without IL-2 and cultured in 96-well plates with or without 1×10^5 NB cells at 1:1 E/T and at a final concentration of 0.5×10^6 CAR$^+$-NKTs/mL. Supernatants were collected after 24 h (9-plex) or 48 h (2-plex) and stored at −80°C until analysis. Supernatants were analyzed using a 2-plex (IL-15 and IL-18) or 9-plex (IL-15, IL-18, IFN-γ, TNF-α, IL-4, IL-6, IL-10, and IL-2) Milliplex Human Cytokine/Chemokine/Growth Factor Panel A magnetic bead panel (HCYTA-60K, Millipore) according to the manufacturer's instructions. Serum samples from mice were collected on day 20 after NKT infusion and stored at −80°C until analysis. Samples were analyzed using a 1-plex (mouse IL-6) Milliplex Mouse Cytokine/Chemokine magnetic bead panel (MCYTOMAG-70K-1, Millipore) and a 9-plex (human IL-18, IL-15, IFN-γ, GM-CSF, G-CSF, IL-4, TNF-α, MIP-1α, and MIP-1β) Milliplex Human Cytokine/Chemokine/Growth Factor Panel A (HCYTA-60K-10, Millipore). To facilitate analysis of samples that had undetectable cytokine/chemokine levels, those samples were assigned a value of half the detection limit specified by the respective kit. All Milliplex assays were analyzed using the Luminex FLEXMAP 3D system with xPONENT software (Luminex) according to the manufacturer's instructions.

In vivo studies

NSG mice were obtained from The Jackson Laboratory and maintained at the Baylor College of Medicine animal care facility. Eight- to 10-week-old mice were injected via tail vein with 1×10^6 FFLUC-expressing CHLA255 or CHLA136 NB cells or CHLA255-WT (for *in vivo* persistence experiments). Seven days later, mice were intravenously infused with 2×10^6, 5×10^6, or 1×10^7 CAR-NKTs. Mice received intraperitoneal (i.p.) injections of IL-2 (2,000 U/mouse) every other day for 2 weeks. Tumor growth was assessed weekly by bioluminescent imaging using an IVIS Lumina III *in vivo* imaging system (Revvity). Where indicated, persistence of FFLUC-GFP$^+$ NKTs was assessed by bioluminescent imaging every other day. Toxicity was assessed by measuring animal weight every other day. Mice were treated i.p. with AP1903 dimerizer (HY-16046, Medchem Express) or vehicle if weight loss was ≥10% of pre-NKT infusion measurements. Blood samples for cytokine and flow-cytometry analyses were collected after AP1903 treatment. After dimerizer or vehicle treatment, spleen samples were collected for further flow-cytometry analyses. To characterize the gene-expression profile of iC9.IL15.IL18 CAR-NKTs *in vivo*, mice were infused with 1×10^6 CHLA255-Luc NB cells via tail vein followed 7 days later by 2×10^6 CAR$^+$-NKTs co-transduced with iC9.IL15.IL18 from two healthy human donors. Mice received i.p. injections of IL-2 (2,000 U/mice) every other day for 2 weeks, and weight was monitored every other day after NKT infusion. Mice receiving CAR-NKTs from the same donor were euthanized when the weight loss average exceeded 10%; at this time, spleens were collected and processed for fluorescence-activated cell sorting (FACS). For *in vivo* infiltration experiments, mice were injected with 1×10^6 CHLA255-WT NB cells via tail vein followed 21 days later by 5×10^6 CAR$^+$-NKTs through the same route. Three days after NKT infusion, mice were euthanized and indicated tissues collected for further processing. Animal experiments were performed according to Institutional Animal Care and Use Committee (IACUC)-approved protocols (Baylor College of Medicine IACUC protocol AN-5194).

Tissue processing for pathology

Tissues from indicated mice were collected in histology cassettes and fixed for 24 h at 4°C in 10% neutral buffered formalin (Epredia, 57-35). Formalin was then replaced with 70% ethanol, and cassettes were kept at 4°C until routine paraffin embedding. IHC staining was performed on 5-μm-thick cut paraffin sections. Heat-induced antigen retrieval conditions for CD3 and TH staining were 0.1 M Tris (pH 9.0) and 10 mM sodium citrate (pH 6.0), respectively. The following primary antibodies were used: hCD3 (1:100 dilution, Agilent, A0452) and TH (1:200 dilution, Leica, NCL-L-TH). Staining was performed using the Agilent Envision+ system HRP-labeled polymer (K4003, anti-rabbit CD3 and K4001, anti-mouse TH). Sections were developed with DAB+ (Agilent, K3468) and counterstained with Harris hematoxylin. Slides were digitized on the Aperio GT-450 whole-slide imaging scanner.

Flow cytometry

Liver and spleen samples were resuspended in 10 mL of Dulbecco's PBS (DPBS) and homogenized using a gentleMACS dissociator and tubes (Miltenyi Biotech). Blood samples were collected via tail vein in heparin-containing tubes (Sigma, H3149-50KU). Dissociated livers were further processed by addition of type V collagenase (Sigma, C9263-500MG, final concentration 1 mg/mL), hyaluronidase (MP Biomedicals, 02100740-CF, final concentration 1 mg/mL), and DNase I (MP Biomedicals, 02100575-CF, final concentration 0.5 mg/mL) followed by a 30-min incubation in a water bath at 37°C. After incubation, liver samples were washed in cold DPBS and processed by resuspension in an isotonic Percoll solution (Cytiva, 45-001-747) as previously described.[85] Liver, spleen, and blood samples were treated with ACK lysis buffer for 5 min at room temperature and washed twice in DPBS. Processed tissue samples or cultured cells were stained with fixable viability dye eFluor 780 (eBioscience, 65-0865-18). NKT phenotype was assessed using the following antibodies: AF488 hCD45 (HI30), PE-Cy7 or BV421 iNKT (6B11), PE-Cy7 CD3 (UCHT1), BV785 CD39 (A1), PE IL18Rα (H44), PeCy7 CD25 (M-A251), PE CD86 (IT2.2), BV421 mouse IgG2a (MOPC-173), BV785 CD62L (DREG-56), PE CXCR4 (12G5), FITC CCR1 (5F10B29), BV650 CXCR3 (G025H7), FITC CX3CR1 (2A9-1), BV421 CCR4 (L291H4, BioLegend), BV480 mouse CD45 (30-F11), BV421 CD62L (DREG-56), BV650 TIM3 (7D3), BUV395 CD4 (SK3), BV421 GD2 (14.G2a), BUV395 iNKT (6B11), BUV805 CD4 (RPA-T4), BV421 CCR8 (433H), BUV563 CCR2 (LS132.1D9), BB700 CXCR6 (13B 1E5), BV421 CCR6 (11A9), PE-Cy7 CCR7 (2-L1-A), PE CCR5 (2D7/CCR5, BD), PE PD-1 (J105), BUV737 LAG3 (3DS223H), PerCP-eFluor-710 TIGIT (MBSA43, eBioscience), and PE-CD34 (QBEND/10, Invitrogen). GD2-CAR expression was evaluated using an AF647

14G2a anti-idiotype 1A7 antibody purified from an 1A7 mouse hybridoma (ATCC, HB-11786), which was custom-conjugated to Alexa Fluor 647 by BioLegend. CD19.CAR and GPC3.CAR expression were evaluated using AF647-FMC63 (200102, Bioswan) and AF647 AffiniPure F(ab′)$_2$ (115-606-003, Jackson ImmunoResearch), respectively. Apoptosis was assessed by staining NKTs with V500 annexin V (561501, BD) in 1× apoptosis buffer (BD) supplemented with 2% FBS for 15 min at room temperature, then washing the cells and resuspending in 1× apoptosis buffer for analysis. Cells were counted using CountBright Plus counting beads (Thermo Fisher, C36995). Analysis was performed on FACSymphony A5 (BD), FACSymphony A1, or iQue 3 (Sartorious) flow cytometers. When indicated, cell sorting was performed using an SH800S cell sorter (Sony Biotechnology). Flow-cytometry data were further analyzed using FlowJo v.10.10 software (BD).

Metabolic status flow cytometry

In brief, NKTs were washed in DPBS, resuspended in fresh NKT medium, and cultured for 30 min at 37°C before adding Mitostatus TMRE (564696, BD) and MG (M7514, Invitrogen) to a final concentration of 10 nM. To assess glucose uptake, NKTs were washed and resuspended in glucose-free RPMI-1640 medium supplemented with GlutaMAX (61870036, Gibco) and incubated for 30 min at 37°C, after which cells were stained with 2-NBDG (Cayman Chemical, 11046) at a final concentration of 50 μM. To assess fatty acid uptake, NKTs were washed in DPBS and resuspended in RPMI-1640 medium supplemented with GlutaMAX and 20 μM of fatty-acid-free BSA (126575, Millipore-Sigma). The cells were then incubated for 30 min at 37°C before staining with BODIPY 500/510 C_1, C_{12} (D3823, Invitrogen) at a final concentration of 0.5 μM. After adding the respective dyes, the cells were further incubated at 37°C for 30 min in darkness, washed twice in DPBS containing 2% FBS, and stained with fixable viability dye 780 and surface antibodies. Samples were then analyzed by flow cytometry as described in the previous section.

Phosphoflow staining

NKTs were washed and resuspended in complete medium (without exogenous IL-2) at 0.25×10^6 NKTs per mL, and 0.5×10^6 cells were plated per well of a 24-well plate. Five days later, the cells were collected and stained with fixable viability dye eFluor 780 at 4°C for 15 min. Cells were then washed in cold PBS and stained for surface markers. NKTs were further processed using the Transcription Factor Phospho set (563239, BD) according to the manufacturer's instructions. In brief, cells were fixed for 1 h at 4°C in 1× Fix-Perm buffer and washed twice in 1× Perm-Wash buffer. Samples were then resuspended in Perm Buffer III (stored at −20°C) and incubated on ice for 20 min. Cells were then washed twice in 1× Perm-Wash buffer and stained overnight at 4°C with PE-pSTAT5 (pY694, 562077, BD) at a 1:15 dilution in 1× Perm-Wash buffer. After an overnight incubation, cells were washed twice with Perm-Wash buffer and resuspended in MACS buffer (DPBS + 0.5% FBS + 1 mM EDTA). Analysis was performed as described in "flow cytometry."

Bulk RNA-seq and data processing

CAR$^+$-NKTs were enriched by FACS after manufacturing and following isolation from mouse spleens. For experiments performed after tumor challenge, we first confirmed tumor elimination by flow cytometry and then enriched live non-apoptotic CAR-NKTs by depletion of annexin V$^+$ cells using the EasySep Dead Cell Removal (Annexin V) kit (STEMCELL Technologies, 17899) following the manufacturer's instructions. Cells were washed, spun down, and lysed in TRI reagent (R2050-1-200, Zymo Research) followed by RNA isolation using the Direct-zol RNA Mini Prep kit (R2053, Zymo Research). Library generation and sequencing were performed by Novogene using a NovaSeq X Plus instrument (Illumina) with 150 bp paired-end read length and around 50 million read pairs per sample. Fastq reads were first trimmed of adapters using Trimmomatic v.0.39 under the default settings using adapters from TruSeq2-PE.fa.[86] Each of the 150-bp paired-end RNA-seq reads for each sample were aligned to the hg38 reference genome using STAR v.2.7.[87] Aligned reads were quantified using FeatureCounts,[88] and differential gene analysis was performed for each CAR condition within each cycle, correcting for donors using DESeq2 v.1.42.1 with a false discovery rate of <0.05.[89] To create heatmaps, significant DEGs were selected and standardized with *Z* scores across samples. Hierarchical clustering and visualization were implemented using ComplexHeatmap.[90] Pathway enrichment was performed using clusterProfiler v.4.10.0[91] through GSEA using signature genes from the C5 ontology gene sets from MSigDB.[92]

scRNA-seq

CAR-NKTs co-transduced with IL-15 or IL-18 from three healthy donors were stimulated 1:1 with CHLA255 NB cells for 3 days as previously described and rested overnight in 200 U/mL IL-2 before dead cells were removed as previously described. A total of 10,000 cells per condition per donor were barcoded, and sequencing libraries were generated using the Chromium GEM-X Single Cell 5′ v3 Gene Expression kit (10× Genomics) following the manufacturer's instructions. Libraries were sequenced by Novogene on an Illumina NovaSeq X Plus instrument with an average read depth of 30,000 reads per cell. The GD2.CAR sequence was incorporated into the GRCh38 human reference genome for data preprocessing and read alignment. Reads were aligned according to the 10× Genomics standard using Cell Ranger (v.8.0.1),[93] and downstream analyses were performed with Seurat (v.5.0.2).[94] We obtained an average of 6.13×10^7 total reads per sample. Cells were classified as CAR positive if they could be aligned to the GD2.CAR sequence. Only cells with raw unique molecular identifier (UMI) counts >0 were used for analysis. Further gene expression and cell filtering were performed under the following exclusion criteria: features with <10 cells, cells with <200 genes, cells with >10% of mitochondrial raw UMIs, and cells with >7,000 genes. Sample integration was performed using Harmony (v.1.2.0).[95] We performed principal-component analysis on scaled data and unsupervised Louvain clustering of CAR$^+$ or total cell populations from IL-18 and IL-15 CAR samples with a resolution of 0.5. Differential gene expression was performed on CAR$^+$ cells to compare clusters by aggregating cells from those clusters and testing

for DEGs. DEG analysis was performed by implementing FindMarkers(min.pct = 0.2, min.cells.feature = 100, test.use = "DESeq2") in Seurat, and DEGs were defined as those with a Benjamini-Hochberg adjusted p value of <0.05. Gene-expression scores and per-cluster GSEA enrichment were performed using gene sets from Hallmark or from predefined gene sets by Miller[96] using AddModuleScore[94] in Seurat. Enrichment analysis was performed with clusterProfiler,[97] and significantly enriched terms were defined as those with a false discovery rate of <0.05.

Metabolic profiling

Unstimulated cryopreserved CAR-NKTs were thawed and rested overnight in medium containing IL-2. Cells were then counted, washed three times in cold DPBS, and counted again, after which 5×10^6 cells were transferred to a microcentrifuge tube to be spun down and frozen. To avoid confounding effects from tumor-generated metabolites, we stimulated CAR-NKTs using plate-bound 1A7 anti-idiotype monoclonal antibody. In brief, non-tissue-culture-treated 24-well plates were coated with 1 μg of 1A7 antibody diluted in PBS at 1 μg/mL, and plates were incubated overnight at 4°C. Plates were then washed with PBS and blocked for 30 min at room temperature using complete NKT medium, after which medium was removed by aspiration. Next, 0.5×10^6 NKTs were loaded into the wells, and the plates were spun down at $400 \times g$ with a low deceleration rate and placed in an incubator. One day later, stimulated NKTs were collected and processed similarly to unstimulated CAR-NKTs. Metabolites were extracted from cell pellets using a liquid-liquid extraction method as previously described.[98–100] Pooled samples were utilized for quality control. In brief, cells were homogenized in a methanol/water (4:1) solution containing an internal standard mix. Following homogenization, chloroform and water were added to facilitate phase separation. Mass spectrometry data were collected using multiple reaction monitoring on a 6495 Triple Quadrupole mass spectrometer coupled to a high-performance liquid chromatography system (Agilent Technologies), operated with Agilent Mass Hunter software.[98–103] Detailed liquid chromatography-mass spectrometry conditions and parameters were consistent with prior studies.[98] Peak integration and data analysis were performed using Agilent Mass Hunter Quantitative Analysis software. The extracted peak areas were $\log_2$ transformed and normalized using isotopically labeled internal standards jasmonic acid, L-tryptophan, and L-zeatin specific to each method. For analysis, each batch of standardized metabolites was analyzed separately by explicitly defining internal batch standards using the estimateSizeFactors[104] function in DESeq2.[89] We tested metabolites from IL-18 versus IL-15 samples either at baseline or after stimulation time points and controlled for donor variation using DESeq(fitType = "local") in DESeq2. We then appended the DEMs' output to their respective condition to examine overall changes in metabolite expression. DEMs were identified using $p < 0.05$ for descriptive visualization purposes. Pathway enrichment analysis was performed using DEMs in the IL-18 versus IL-15 group with the Enrichment Analysis tool from MetaboAnalyst.[105]

Seahorse assays

Mitochondrial respiration and glycolysis were measured using Mito Stress Test XF (103015-100, Agilent) and Glycolysis Stress Test XF (103020-100, Agilent) kits in a Seahorse XFe96 instrument (Agilent) following the manufacturer's instructions. Cartridge hydration, equilibration and loading, and plate coating in Cell-Tak (354240, Corning) were performed as indicated by Agilent. In brief, 1 day before setting up the assay, 3×10^6 CAR^+-NKTs per condition and donor were washed in DPBS and resuspended in fresh NKT medium supplemented with 200 U/mL IL-2 at a final concentration of 0.5×10^6 CAR^+-NKTs/mL in a well of a 24-well G-Rex device. On the following day, cells were washed twice in DPBS and once more in the respective assay medium. Cells were then resuspended in a low volume of respective assay medium, counted, and diluted to a concentration of 5×10^6 cells/mL in assay medium. When indicated by the manufacturer's protocol, 50 μL of cell suspension (0.25×10^6 cells) was added to the respective wells of a Seahorse plate coated in Cell-Tak. Thereafter, plates were spun down at $400 \times g$ without braking to ensure an even cell distribution on the surface of the wells. Other steps, including amounts of compounds specific for mito- or glyco-stress tests, were performed as indicated by the manufacturer. Metabolic parameters were calculated using Seahorse Wave software.

Statistics

For *in vitro* or *in vivo* experiments comparing two groups, two-tailed paired or unpaired t tests were used. When comparing more than two groups, unpaired or paired ANOVA with Tukey's or Dunnett's multiple-comparison tests were used. Survival curves were compared using the log-rank Mantel-Cox test. Statistical methods were not used to predetermine sample sizes. Unless otherwise indicated, statistical analyses were calculated using GraphPad Prism v.10.4.1.

DATA AND CODE AVAILABILITY

Raw bulk and scRNA-seq data and raw metabolomics data are available from the corresponding author upon request.

ACKNOWLEDGMENTS

This work was supported by NIH National Cancer Institute grants R01-CA262250 (L.S.M.), P50-CA126752 (Project 1, L.S.M.), and R01-CA247436 (G.D.), as well as the Isabella Santos Foundation (L.S.M.). The authors are grateful for the excellent technical assistance provided by the staff at the Flow Cytometry Core Laboratory of the Texas Children's Cancer and Hematology Center, Small Animal Imaging Core facility at Texas Children's Hospital, the Metabolomics Core (CPRIT-RP210227 and NIH P30 CA125123), and the Breast Center Pathology Core (NIH 1S10D028671-01, G.M.) at Baylor College of Medicine. Illustrations were edited and generated using Inkscape software, and some illustrations were obtained from the NIAID Visual & Medical Arts BIOART source.

AUTHOR CONTRIBUTIONS

Conceptualization, G.A.B.B., G.D., and L.S.M.; methodology, G.A.B.B., E.L., G.T., X.R., X.X., A.N.C., G.D., and L.S.M.; investigation, G.A.B.B., E.L., K.D., P.H., L.D.C.G., Y.W., B.Y., L.G., M.S.W., J.J., Y.-H.L., A.A., N.W., S.M., and G.M.; formal analysis, G.A.B.B., D.A.d.l.C., and G.M.; writing – original draft, G.B.B. and L.S.M.; writing – review & editing, G.A.B.B., A.N.C., E.J.D.P., and L.S.M.; visualization, G.A.B.B. and D.A.C.

DECLARATION OF INTERESTS

G.A.B.B., A.N.C., and L.S.M. are co-inventors on a pending patent application relevant to this work.

SUPPLEMENTAL INFORMATION

Supplemental information can be found online at https://doi.org/10.1016/j.ymthe.2026.01.001.

REFERENCES

1. Albelda, S.M. (2024). CAR T cell therapy for patients with solid tumours: key lessons to learn and unlearn. Nat. Rev. Clin. Oncol. *21*, 47–66. https://doi.org/10.1038/s41571-023-00832-4.
2. Hou, A.J., Chen, L.C., and Chen, Y.Y. (2021). Navigating CAR-T cells through the solid-tumour microenvironment. Nat. Rev. Drug Discov. *20*, 531–550. https://doi.org/10.1038/s41573-021-00189-2.
3. Metelitsa, L.S., Wu, H.-W., Wang, H., Yang, Y., Warsi, Z., Asgharzadeh, S., Groshen, S., Wilson, S.B., and Seeger, R.C. (2004). Natural killer T cells infiltrate neuroblastomas expressing the chemokine CCL2. J. Exp. Med. *199*, 1213–1221.
4. Malmberg, K.-J., Carlsten, M., Björklund, A., Sohlberg, E., Bryceson, Y.T., and Ljunggren, H.-G. (2017). Natural killer cell-mediated immunosurveillance of human cancer. Semin. Immunol. *31*, 20–29. https://doi.org/10.1016/j.smim.2017.08.002.
5. Silva-Santos, B., Mensurado, S., and Coffelt, S.B. (2019). γδ T cells: pleiotropic immune effectors with therapeutic potential in cancer. Nat. Rev. Cancer *19*, 392–404. https://doi.org/10.1038/s41568-019-0153-5.
6. Courtney, A.N., Tian, G., and Metelitsa, L.S. (2023). Natural killer T cells and other innate-like T lymphocytes as emerging platforms for allogeneic cancer cell therapy. Blood *141*, 869–876. https://doi.org/10.1182/blood.2022016201.
7. Heczey, A., Liu, D., Tian, G., Courtney, A.N., Wei, J., Marinova, E., Gao, X., Guo, L., Yvon, E., Hicks, J., et al. (2014). Invariant NKT cells with chimeric antigen receptor provide a novel platform for safe and effective cancer immunotherapy. Blood *124*, 2824–2833. https://doi.org/10.1182/blood-2013-11-541235.
8. Makkouk, A., Yang, X.C., Barca, T., Lucas, A., Turkoz, M., Wong, J.T.S., Nishimoto, K.P., Brodey, M.M., Tabrizizad, M., Gundurao, S.R.Y., et al. (2021). Off-the-shelf Vδ1 gamma delta T cells engineered with glypican-3 (GPC-3)-specific chimeric antigen receptor (CAR) and soluble IL-15 display robust antitumor efficacy against hepatocellular carcinoma. J. Immunother. Cancer *9*, e003441. https://doi.org/10.1136/jitc-2021-003441.
9. Dogan, M., Karhan, E., Kozhaya, L., Placek, L., Chen, X., Yigit, M., and Unutmaz, D. (2022). Engineering Human MAIT Cells with Chimeric Antigen Receptors for Cancer Immunotherapy. J. Immunol. *209*, 1523–1531. https://doi.org/10.4049/jimmunol.2100856.
10. Li, Y., Basar, R., Wang, G., Liu, E., Moyes, J.S., Li, L., Kerbauy, L.N., Uprety, N., Fathi, M., Rezvan, A., et al. (2022). KIR-based inhibitory CARs overcome CAR-NK cell trogocytosis-mediated fratricide and tumor escape. Nat. Med. *28*, 2133–2144. https://doi.org/10.1038/s41591-022-02003-x.
11. Courtney, A.N., Zhou, X., Tian, G., Wang, Y., Metelitsa, L.S., and Dotti, G. (2025). Facts and Hopes of Chimeric Antigen Receptor–Redirected NK T Cells. Clin. Cancer Res. *31*, 5137–5144. https://doi.org/10.1158/1078-0432.CCR-25-0197.
12. Zhou, X., Wang, Y., Dou, Z., Delfanti, G., Tsahouridis, O., Pellegry, C.M., Zingarelli, M., Atassi, G., Woodcock, M.G., Casorati, G., et al. (2024). CAR-redirected natural killer T cells demonstrate superior antitumor activity to CAR-T cells through multimodal CD1d-dependent mechanisms. Nat. Cancer *5*, 1607–1621. https://doi.org/10.1038/s43018-024-00830-0.
13. Song, L., Asgharzadeh, S., Salo, J., Engell, K., Wu, H.w., Sposto, R., Ara, T., Silverman, A.M., DeClerck, Y.A., Seeger, R.C., and Metelitsa, L.S. (2009). Vα24-invariant NKT cells mediate antitumor activity via killing of tumor-associated macrophages. J. Clin. Invest. *119*, 1524–1536. https://doi.org/10.1172/JCI37869.
14. Cortesi, F., Delfanti, G., Grilli, A., Calcinotto, A., Gorini, F., Pucci, F., Lucianò, R., Grioni, M., Recchia, A., Benigni, F., et al. (2018). Bimodal CD40/Fas-Dependent Crosstalk between iNKT Cells and Tumor-Associated Macrophages Impairs Prostate Cancer Progression. Cell Rep. *22*, 3006–3020. https://doi.org/10.1016/j.celrep.2018.02.058.
15. Delfanti, G., Cortesi, F., Perini, A., Antonini, G., Azzimonti, L., de Lalla, C., Garavaglia, C., Squadrito, M.L., Fedeli, M., Consonni, M., et al. (2022). TCR-engineered iNKT cells induce robust antitumor response by dual targeting cancer and suppressive myeloid cells. Sci. Immunol. *7*, eabn6563. https://doi.org/10.1126/sciimmunol.abn6563.
16. Simonetta, F., Lohmeyer, J.K., Hirai, T., Maas-Bauer, K., Alvarez, M., Wenokur, A.S., Baker, J., Aalipour, A., Ji, X., Haile, S., et al. (2021). Allogeneic CAR Invariant Natural Killer T Cells Exert Potent Antitumor Effects through Host CD8 T-Cell Cross-Priming. Clin. Cancer Res. *27*, 6054–6064. https://doi.org/10.1158/1078-0432.CCR-21-1329.
17. Tachibana, T., Onodera, H., Tsuruyama, T., Mori, A., Nagayama, S., Hiai, H., and Imamura, M. (2005). Increased intratumor Vα24-positive natural killer T cells: a prognostic factor for primary colorectal carcinomas. Clin. Cancer Res. *11*, 7322–7327.
18. Avanzi, M.P., Yeku, O., Li, X., Wijewarnasuriya, D.P., van Leeuwen, D.G., Cheung, K., Park, H., Purdon, T.J., Daniyan, A.F., Spitzer, M.H., and Brentjens, R.J. (2018). Engineered Tumor-Targeted T Cells Mediate Enhanced Anti-Tumor Efficacy Both Directly and through Activation of the Endogenous Immune System. Cell Rep. *23*, 2130–2141. https://doi.org/10.1016/j.celrep.2018.04.051.
19. Poels, R., Drent, E., Lameris, R., Katsarou, A., Themeli, M., van der Vliet, H.J., de Gruijl, T.D., van de Donk, N.W.C.J., and Mutis, T. (2021). Preclinical Evaluation of Invariant Natural Killer T Cells Modified with CD38 or BCMA Chimeric Antigen Receptors for Multiple Myeloma. Int. J. Mol. Sci. *22*, 1096. https://doi.org/10.3390/ijms22031096.
20. O'Neal, J., Cooper, M.L., Ritchey, J.K., Gladney, S., Niswonger, J., González, L.S., Street, E., Haas, G.J., Carter, A., Amayta, P.N., et al. (2023). Anti-myeloma efficacy of CAR-iNKT is enhanced with a long-acting IL-7, rhIL-7-hyFc. Blood Adv. *7*, 6009–6022. https://doi.org/10.1182/bloodadvances.2023010032.
21. Liu, Y., Dang, Y., Zhang, C., Liu, L., Cai, W., Li, L., Fang, L., Wang, M., Xu, S., Wang, G., et al. (2024). IL-21-armored B7H3 CAR-iNKT cells exert potent antitumor effects. iScience *27*, 108597. https://doi.org/10.1016/j.isci.2023.108597.
22. Hatae, R., Watchmaker, P.B., Yamamichi, A., Kyewalabye, K., Okada, K., Phyu, S., Goretsky, Y., Haegelin, J., Pineo-Cavanaugh, P., Gallus, M., et al. (2025). Comparative evaluation of CAR-expressing T-NK-NKT-cells, and macrophages in an immunocompetent mouse glioma model. Neurooncol. Adv. *7*, vdaf074. https://doi.org/10.1093/noajnl/vdaf074.
23. Ren, H., Elliott, N., Lye, B., Sharif Shohan, M.U., Cross, J.W., Field, L., Ponnusamy, K., Rice, S., Jackson, T., Leontari, I., et al. (2026). Off-the-shelf dual CAR-iNKT cell immunotherapy eradicates medullary and leptomeningeal high-risk *KMT2A*-rearranged leukemia. Blood *147*, 180–196. https://doi.org/10.1182/blood.2025029302.
24. Herd, F., Basta, N.O., McNally, R.J.Q., and Tweddle, D.A. (2019). A systematic review of re-induction chemotherapy for children with relapsed high-risk neuroblastoma. Eur. J. Cancer *111*, 50–58. https://doi.org/10.1016/j.ejca.2018.12.032.
25. DuBois, S.G., Macy, M.E., and Henderson, T.O. (2022). High-Risk and Relapsed Neuroblastoma: Toward More Cures and Better Outcomes. Am. Soc. Clin. Oncol. Educ. Book. *42*, 1–13. https://doi.org/10.1200/EDBK_349783.
26. Dhillon, S. (2015). Dinutuximab: First Global Approval. Drugs *75*, 923–927. https://doi.org/10.1007/s40265-015-0399-5.
27. Markham, A. (2021). Naxitamab: First Approval. Drugs *81*, 291–296. https://doi.org/10.1007/s40265-021-01467-4.
28. Pule, M.A., Savoldo, B., Myers, G.D., Rossig, C., Russell, H.V., Dotti, G., Huls, M.H., Liu, E., Gee, A.P., Mei, Z., et al. (2008). Virus-specific T cells engineered to coexpress tumor-specific receptors: persistence and antitumor activity in individuals with neuroblastoma. Nat. Med. *14*, 1264–1270. https://doi.org/10.1038/nm.1882.
29. Heczey, A., Louis, C.U., Savoldo, B., Dakhova, O., Durett, A., Grilley, B., Liu, H., Wu, M.F., Mei, Z., Gee, A., et al. (2017). CAR T Cells Administered in Combination with Lymphodepletion and PD-1 Inhibition to Patients with Neuroblastoma. Mol. Ther. *25*, 2214–2224. https://doi.org/10.1016/j.ymthe.2017.05.012.
30. Heczey, A., Xu, X., Courtney, A.N., Tian, G., Barragan, G.A., Guo, L., Amador, C.M., Ghatwai, N., Rathi, P., Wood, M.S., et al. (2023). Anti-GD2 CAR-NKT cells in relapsed or refractory neuroblastoma: updated phase 1 trial interim results. Nat. Med. *29*, 1379–1388. https://doi.org/10.1038/s41591-023-02363-y.
31. Xu, X., Huang, W., Heczey, A., Liu, D., Guo, L., Wood, M., Jin, J., Courtney, A.N., Liu, B., Di Pierro, E.J., et al. (2019). NKT Cells Coexpressing a GD2-Specific

Chimeric Antigen Receptor and IL15 Show Enhanced In Vivo Persistence and Antitumor Activity against Neuroblastoma. Clin. Cancer Res. *25*, 7126–7138. https://doi.org/10.1158/1078-0432.CCR-19-0421.

32. Landoni, E., Woodcock, M.G., Barragan, G., Casirati, G., Cinella, V., Stucchi, S., Flick, L.M., Withers, T.A., Hudson, H., Casorati, G., et al. (2024). IL-12 reprograms CAR-expressing natural killer T cells to long-lived Th1-polarized cells with potent antitumor activity. Nat. Commun. *15*, 89. https://doi.org/10.1038/s41467-023-44310-y.

33. Cirella, A., Olivera, I., Luri-Rey, C., Bolaños, E., Berraondo, P., and Melero, I. (2023). Interleukin-18 in cancer immunology and immunotherapy. Expert Opin. Ther. Targets *27*, 1035–1042. https://doi.org/10.1080/14728222.2023.2287574.

34. Leite-de-Moraes, M.C., Hameg, A., Pacilio, M., Koezuka, Y., Taniguchi, M., Van Kaer, L., Schneider, E., Dy, M., and Herbelin, A. (2001). IL-18 Enhances IL-4 Production by Ligand-Activated NKT Lymphocytes: A Pro-Th2 Effect of IL-18 Exerted Through NKT Cells1. J. Immunol. *166*, 945–951. https://doi.org/10.4049/jimmunol.166.2.945.

35. Baxevanis, C.N., Gritzapis, A.D., and Papamichail, M. (2003). In Vivo Antitumor Activity of NKT Cells Activated by the Combination of IL-12 and IL-18 1. J. Immunol. *171*, 2953–2959. https://doi.org/10.4049/jimmunol.171.6.2953.

36. Hu, B., Ren, J., Luo, Y., Keith, B., Young, R.M., Scholler, J., Zhao, Y., and June, C.H. (2017). Augmentation of Antitumor Immunity by Human and Mouse CAR T Cells Secreting IL-18. Cell Rep. *20*, 3025–3033. https://doi.org/10.1016/j.celrep.2017.09.002.

37. Chmielewski, M., and Abken, H. (2017). CAR T Cells Releasing IL-18 Convert to T-Bethigh FoxO1low Effectors that Exhibit Augmented Activity against Advanced Solid Tumors. Cell Rep. *21*, 3205–3219. https://doi.org/10.1016/j.celrep.2017.11.063.

38. Jaspers, J.E., Khan, J.F., Godfrey, W.D., Lopez, A.V., Ciampricotti, M., Rudin, C.M., and Brentjens, R.J. (2023). IL-18–secreting CAR T cells targeting DLL3 are highly effective in small cell lung cancer models. J. Clin. Invest. *133*, e166028. https://doi.org/10.1172/JCI166028.

39. Ng, B.D., Rajagopalan, A., Kousa, A.I., Fischman, J.S., Chen, S., Massa, A., Elias, H.K., Manuele, D., Galiano, M., Lemarquis, A.L., et al. (2024). IL-18-secreting multiantigen targeting CAR T cells eliminate antigen-low myeloma in an immunocompetent mouse model. Blood *144*, 171–186. https://doi.org/10.1182/blood.2023022293.

40. Fischer-Riepe, L., Kailayangiri, S., Zimmermann, K., Pfeifer, R., Aigner, M., Altvater, B., Kretschmann, S., Völkl, S., Hartley, J., Dreger, C., et al. (2024). Preclinical Development of CAR T Cells with Antigen-Inducible IL18 Enforcement to Treat GD2-Positive Solid Cancers. Clin. Cancer Res. *30*, 3564–3577. https://doi.org/10.1158/1078-0432.CCR-23-3157.

41. Hull, C.M., Larcombe-Young, D., Mazza, R., George, M., Davies, D.M., Schurich, A., and Maher, J. (2024). Granzyme B-activated IL18 potentiates αβ and γδ CAR T cell immunotherapy in a tumor-dependent manner. Mol. Ther. *32*, 2373–2392. https://doi.org/10.1016/j.ymthe.2024.05.013.

42. Svoboda, J., Landsburg, D.J., Gerson, J., Nasta, S.D., Barta, S.K., Chong, E.A., Cook, M., Frey, N.V., Shea, J., Cervini, A., et al. (2025). Enhanced CAR T-Cell Therapy for Lymphoma after Previous Failure. N. Engl. J. Med. *392*, 1824–1835. https://doi.org/10.1056/NEJMoa2408771.

43. Geyer, M.B., DeWolf, S., Mi, X., Weis, K., Shaffer, B.C., Cadzin, B., McAvoy, D., Katsamakis, Z., Lorenc, R., Lewis, A.M., et al. (2025). CD371-Targeted CAR T-cells Secreting Interleukin-18 Exhibit Robust Expansion and Clear Refractory Acute Myeloid Leukemia. Blood *146*, 3163–3174. https://doi.org/10.1182/blood.2025029532.

44. Fujibayashi, Y., Fujimori, Y., Kasumoto, I., Kai, S., Hara, H., Okamura, H., Tsutsui, H., Ogawa, H., and Nakanishi, K. (2007). Interleukin-18 regulates T helper 1 or 2 immune responses of human cord blood CD4+ Vα24+Vβ11+ natural killer T cells. Int. J. Mol. Med. *20*, 241–245. https://doi.org/10.3892/ijmm.20.2.241.

45. Lind, S.M., Kuylenstierna, C., Moll, M., Jordö, E.D., Winqvist, O., Lundeberg, L., Karlsson, M.A., Linder, M.T., Johansson, C., Scheynius, A., et al. (2009). IL-18 skews the invariant NKT-cell population via autoreactive activation in atopic eczema. Eur. J. Immunol. *39*, 2293–2301. https://doi.org/10.1002/eji.200839195.

46. Di Stasi, A., Tey, S.-K., Dotti, G., Fujita, Y., Kennedy-Nasser, A., Martinez, C., Straathof, K., Liu, E., Durett, A.G., Grilley, B., et al. (2011). Inducible Apoptosis as a Safety Switch for Adoptive Cell Therapy. N. Engl. J. Med. *365*, 1673–1683. https://doi.org/10.1056/NEJMoa1106152.

47. Quach, D.H., Becerra-Dominguez, L., Rouce, R.H., and Rooney, C.M. (2019). A strategy to protect off-the-shelf cell therapy products using virus-specific T-cells engineered to eliminate alloreactive T-cells. J. Transl. Med. *17*, 240. https://doi.org/10.1186/s12967-019-1988-y.

48. Ngai, H., Tian, G., Courtney, A.N., Ravari, S.B., Guo, L., Liu, B., Jin, J., Shen, E.T., Di Pierro, E.J., and Metelitsa, L.S. (2018). IL-21 Selectively Protects CD62L+ NKT Cells and Enhances Their Effector Functions for Adoptive Immunotherapy. J. Immunol. *201*, 2141–2153. https://doi.org/10.4049/jimmunol.1800429.

49. Wang, X., and Zhao, X.-Y. (2021). Transcription Factors Associated With IL-15 Cytokine Signaling During NK Cell Development. Front. Immunol. *12*, 610789. https://doi.org/10.3389/fimmu.2021.610789.

50. Rex, D.A.B., Agarwal, N., Prasad, T.S.K., Kandasamy, R.K., Subbannayya, Y., and Pinto, S.M. (2020). A comprehensive pathway map of IL-18-mediated signalling. J. Cell Commun. Signal. *14*, 257–266. https://doi.org/10.1007/s12079-019-00544-4.

51. Tian, G., Courtney, A.N., Jena, B., Heczey, A., Liu, D., Marinova, E., Guo, L., Xu, X., Torikai, H., Mo, Q., et al. (2016). CD62L+ NKT cells have prolonged persistence and antitumor activity in vivo. J. Clin. Invest. *126*, 2341–2355. https://doi.org/10.1172/JCI83476.

52. Ngai, H., Barragan, G.A., Tian, G., Balzeau, J.C., Zhang, C., Courtney, A.N., Guo, L., Xu, X., Wood, M.S., Drabek, J.M., et al. (2023). LEF1 Drives a Central Memory Program and Supports Antitumor Activity of Natural Killer T Cells. Cancer Immunol. Res. *11*, 171–183. https://doi.org/10.1158/2326-6066.CIR-22-0333.

53. Mabe, N.W., Huang, M., Dalton, G.N., Alexe, G., Schaefer, D.A., Geraghty, A.C., Robichaud, A.L., Conway, A.S., Khalid, D., Mader, M.M., et al. (2022). Transition to a mesenchymal state in neuroblastoma confers resistance to anti-GD2 antibody via reduced expression of ST8SIA1. Nat. Cancer *3*, 976–993. https://doi.org/10.1038/s43018-022-00405-x.

54. Warren, M., Matsuno, R., Tran, H., and Shimada, H. (2018). Utility of Phox2b immunohistochemical stain in neural crest tumours and non-neural crest tumours in paediatric patients. Histopathology *72*, 685–696. https://doi.org/10.1111/his.13412.

55. Wang, R., Dillon, C.P., Shi, L.Z., Milasta, S., Carter, R., Finkelstein, D., McCormick, L.L., Fitzgerald, P., Chi, H., Munger, J., and Green, D.R. (2011). The transcription factor Myc controls metabolic reprogramming upon T lymphocyte activation. Immunity *35*, 871–882. https://doi.org/10.1016/j.immuni.2011.09.021.

56. Chi, H. (2012). Regulation and function of mTOR signalling in T cell fate decisions. Nat. Rev. Immunol. *12*, 325–338. https://doi.org/10.1038/nri3198.

57. Shanley, M., Daher, M., Dou, J., Li, S., Basar, R., Rafei, H., Dede, M., Gumin, J., Pantaleón García, J., Nunez Cortes, A.K., et al. (2024). Interleukin-21 engineering enhances NK cell activity against glioblastoma via CEBPD. Cancer Cell *42*, 1450–1466.e11. https://doi.org/10.1016/j.ccell.2024.07.007.

58. Delconte, R.B., Kolesnik, T.B., Dagley, L.F., Rautela, J., Shi, W., Putz, E.M., Stannard, K., Zhang, J.-G., Teh, C., Firth, M., et al. (2016). CIS is a potent checkpoint in NK cell–mediated tumor immunity. Nat. Immunol. *17*, 816–824. https://doi.org/10.1038/ni.3470.

59. Liu, X., and Peng, G. (2021). Mitochondria orchestrate T cell fate and function. Nat. Immunol. *22*, 276–278. https://doi.org/10.1038/s41590-020-00861-6.

60. Zhao, Y., Chen, J., Andreatta, M., Feng, B., Xie, Y.-Q., Wenes, M., Wang, Y., Gao, M., Hu, X., Romero, P., et al. (2024). IL-10-expressing CAR T cells resist dysfunction and mediate durable clearance of solid tumors and metastases. Nat. Biotechnol. *42*, 1693–1704. https://doi.org/10.1038/s41587-023-02060-8.

61. Carr, E.L., Kelman, A., Wu, G.S., Gopaul, R., Senkevitch, E., Aghvanyan, A., Turay, A.M., and Frauwirth, K.A. (2010). Glutamine Uptake and Metabolism Are Coordinately Regulated by ERK/MAPK During T Lymphocyte Activation. J. Immunol. *185*, 1037–1044. https://doi.org/10.4049/jimmunol.0903586.

62. Klysz, D.D., Fowler, C., Malipatlolla, M., Stuani, L., Freitas, K.A., Chen, Y., Meier, S., Daniel, B., Sandor, K., Xu, P., et al. (2024). Inosine induces stemness features in CAR-T cells and enhances potency. Cancer Cell *42*, 266–282.e8. https://doi.org/10.1016/j.ccell.2024.01.002.

63. Wang, T., Gnanaprakasam, J.N.R., Chen, X., Kang, S., Xu, X., Sun, H., Liu, L., Rodgers, H., Miller, E., Cassel, T.A., et al. (2020). Inosine is an alternative carbon source for CD8+-T-cell function under glucose restriction. Nat. Metab. *2*, 635–647. https://doi.org/10.1038/s42255-020-0219-4.

64. Quéméneur, L., Gerland, L.-M., Flacher, M., Ffrench, M., Revillard, J.-P., and Genestier, L. (2003). Differential Control of Cell Cycle, Proliferation, and Survival of Primary T Lymphocytes by Purine and Pyrimidine Nucleotides1. J. Immunol. *170*, 4986–4995. https://doi.org/10.4049/jimmunol.170.10.4986.

65. Fairbanks, L.D., Bofill, M., Ruckemann, K., and Simmonds, H.A. (1995). Importance of Ribonucleotide Availability to Proliferating T-lymphocytes from Healthy Humans: Disproportionate Expansion of Pyrimidine Pools and Contrasting Effects of De Novo Synthesis Inhibitors. J. Biol. Chem. *270*, 29682–29689. https://doi.org/10.1074/jbc.270.50.29682.

66. Steffin, D., Ghatwai, N., Montalbano, A., Rathi, P., Courtney, A.N., Arnett, A.B., Fleurence, J., Sweidan, R., Wang, T., Zhang, H., et al. (2025). Interleukin-15-armoured GPC3 CAR T cells for patients with solid cancers. Nature *637*, 940–946. https://doi.org/10.1038/s41586-024-08261-8.

67. Dong, C. (2021). Cytokine Regulation and Function in T Cells. Annu. Rev. Immunol. *39*, 51–76. https://doi.org/10.1146/annurev-immunol-061020-053702.

68. Rochman, Y., Spolski, R., and Leonard, W.J. (2009). New insights into the regulation of T cells by γc family cytokines. Nat. Rev. Immunol. *9*, 480–490. https://doi.org/10.1038/nri2580.

69. Terzic, T., Cordeau, M., Herblot, S., Teira, P., Cournoyer, S., Beaunoyer, M., Peuchmaur, M., Duval, M., and Sartelet, H. (2018). Expression of Disialoganglioside (GD2) in Neuroblastic Tumors: A Prognostic Value for Patients Treated With Anti-GD2 Immunotherapy. Pediatr. Dev. Pathol. *21*, 355–362. https://doi.org/10.1177/1093526617723972.

70. French, A.R., Holroyd, E.B., Yang, L., Kim, S., and Yokoyama, W.M. (2006). IL-18 acts synergistically with IL-15 in stimulating natural killer cell proliferation. Cytokine *35*, 229–234. https://doi.org/10.1016/j.cyto.2006.08.006.

71. Strengell, M., Matikainen, S., Sirén, J., Lehtonen, A., Foster, D., Julkunen, I., and Sareneva, T. (2003). IL-21 in Synergy with IL-15 or IL-18 Enhances IFN-γ Production in Human NK and T Cells1. J. Immunol. *170*, 5464–5469. https://doi.org/10.4049/jimmunol.170.11.5464.

72. Li, H.-S., Israni, D.V., Gagnon, K.A., Gan, K.A., Raymond, M.H., Sander, J.D., Roybal, K.T., Joung, J.K., Wong, W.W., and Khalil, A.S. (2022). Multidimensional control of therapeutic human cell function with synthetic gene circuits. Science *378*, 1227–1234. https://doi.org/10.1126/science.ade0156.

73. Chen, A.X.Y., Yap, K.M., Kim, J.S., Sek, K., Huang, Y.-K., Dunbar, P.A., Wiebking, V., Armitage, J.D., Munoz, I., Todd, K.L., et al. (2025). Rewiring endogenous genes in CAR T cells for tumour-restricted payload delivery. Nature *644*, 241–251. https://doi.org/10.1038/s41586-025-09212-7.

74. Svoboda, J., Landsburg, D.J., Nasta, S.D., Barta, S.K., Chong, E.A., Lariviere, M.J., Shea, J., Cervini, A., Hexner, E.O., Marshall, A., et al. (2024). Safety and efficacy of armored huCART19-IL18 in patients with relapsed/refractory lymphomas that progressed after anti-CD19 CAR T cells. J. Clin. Oncol. *42*, 7004. https://doi.org/10.1200/JCO.2024.42.16_suppl.7004.

75. Feng, B., Li, R., Li, W., and Tang, L. (2024). Metabolic immunoengineering approaches to enhance CD8+ T cell-based cancer immunotherapy. Cell Syst. *15*, 1225–1244. https://doi.org/10.1016/j.cels.2024.11.010.

76. Corrado, M., and Pearce, E.L. (2022). Targeting memory T cell metabolism to improve immunity. J. Clin. Invest. *132*, e148546. https://doi.org/10.1172/JCI148546.

77. Chen, Y., Sun, C., Landoni, E., Metelitsa, L., Dotti, G., and Savoldo, B. (2019). Eradication of Neuroblastoma by T Cells Redirected with an Optimized GD2-Specific Chimeric Antigen Receptor and Interleukin-15. Clin. Cancer Res. *25*, 2915–2924. https://doi.org/10.1158/1078-0432.CCR-18-1811.

78. Vera, J., Savoldo, B., Vigouroux, S., Biagi, E., Pule, M., Rossig, C., Wu, J., Heslop, H.E., Rooney, C.M., Brenner, M.K., and Dotti, G. (2006). T lymphocytes redirected against the κ light chain of human immunoglobulin efficiently kill mature B lymphocyte-derived malignant cells. Blood *108*, 3890–3897. https://doi.org/10.1182/blood-2006-04-017061.

79. Li, W., Guo, L., Rathi, P., Marinova, E., Gao, X., Wu, M.-F., Liu, H., Dotti, G., Gottschalk, S., Metelitsa, L.S., et al. (2017). Redirecting T Cells to Glypican-3 with 4-1BB Zeta Chimeric Antigen Receptors Results in Th1 Polarization and Potent Antitumor Activity. Hum. Gene Ther. *28*, 437–448. https://doi.org/10.1089/hum.2016.025.

80. Rivière, I., Brose, K., and Mulligan, R.C. (1995). Effects of retroviral vector design on expression of human adenosine deaminase in murine bone marrow transplant recipients engrafted with genetically modified cells. Proc. Natl. Acad. Sci. USA *92*, 6733–6737. https://doi.org/10.1073/pnas.92.15.6733.

81. Straathof, K.C., Pulè, M.A., Yotnda, P., Dotti, G., Vanin, E.F., Brenner, M.K., Heslop, H.E., Spencer, D.M., and Rooney, C.M. (2005). An inducible caspase 9 safety switch for T-cell therapy. Blood *105*, 4247–4254. https://doi.org/10.1182/blood-2004-11-4564.

82. Jutz, S., Hennig, A., Paster, W., Asrak, Ö., Dijanovic, D., Kellner, F., Pickl, W.F., Huppa, J.B., Leitner, J., and Steinberger, P. (2017). A cellular platform for the evaluation of immune checkpoint molecules. Oncotarget *8*, 64892–64906. https://doi.org/10.18632/oncotarget.17615.

83. Pulè, M.A., Straathof, K.C., Dotti, G., Heslop, H.E., Rooney, C.M., and Brenner, M.K. (2005). A chimeric T cell antigen receptor that augments cytokine release and supports clonal expansion of primary human T cells. Mol. Ther. *12*, 933–941. https://doi.org/10.1016/j.ymthe.2005.04.016.

84. Tian, G., Barragán, G.A., Yu, H., Martinez-Amador, C., Adaikkalavan, A., Rios, X., Guo, L., Drabek, J.M., Pardias, O., Xu, X., et al. (2025). PRDM1 is a key regulator of the natural killer T–cell central memory program and effector function. Cancer Immunol. Res. https://doi.org/10.1158/2326-6066.CIR-24-0259.

85. Li, X., Tsuji, M., Schneck, J., and Webb, T.J. (2013). Generation of Mouse iNKT Cell Lines. Bio. Protoc. *3*, e419.

86. Bolger, A.M., Lohse, M., and Usadel, B. (2014). Trimmomatic: a flexible trimmer for Illumina sequence data. Bioinformatics *30*, 2114–2120. https://doi.org/10.1093/bioinformatics/btu170.

87. Dobin, A., Davis, C.A., Schlesinger, F., Drenkow, J., Zaleski, C., Jha, S., Batut, P., Chaisson, M., and Gingeras, T.R. (2013). STAR: ultrafast universal RNA-seq aligner. Bioinformatics *29*, 15–21. https://doi.org/10.1093/bioinformatics/bts635.

88. Liao, Y., Smyth, G.K., and Shi, W. (2014). featureCounts: an efficient general purpose program for assigning sequence reads to genomic features. Bioinformatics *30*, 923–930. https://doi.org/10.1093/bioinformatics/btt656.

89. Love, M.I., Huber, W., and Anders, S. (2014). Moderated estimation of fold change and dispersion for RNA-seq data with DESeq2. Genome Biol. *15*, 550. https://doi.org/10.1186/s13059-014-0550-8.

90. Gu, Z. (2022). Complex heatmap visualization. iMeta *1*, e43. https://doi.org/10.1002/imt2.43.

91. Yu, G., Wang, L.-G., Han, Y., and He, Q.-Y. (2012). clusterProfiler: an R Package for Comparing Biological Themes Among Gene Clusters. OMICS J. Integr. Biol. *16*, 284–287. https://doi.org/10.1089/omi.2011.0118.

92. Subramanian, A., Tamayo, P., Mootha, V.K., Mukherjee, S., Ebert, B.L., Gillette, M.A., Paulovich, A., Pomeroy, S.L., Golub, T.R., Lander, E.S., and Mesirov, J.P. (2005). Gene set enrichment analysis: A knowledge-based approach for interpreting genome-wide expression profiles. Proc. Natl. Acad. Sci. USA *102*, 15545–15550. https://doi.org/10.1073/pnas.0506580102.

93. Zheng, G.X.Y., Terry, J.M., Belgrader, P., Ryvkin, P., Bent, Z.W., Wilson, R., Ziraldo, S.B., Wheeler, T.D., McDermott, G.P., Zhu, J., et al. (2017). Massively parallel digital transcriptional profiling of single cells. Nat. Commun. *8*, 14049. https://doi.org/10.1038/ncomms14049.

94. Hao, Y., Stuart, T., Kowalski, M.H., Choudhary, S., Hoffman, P., Hartman, A., Srivastava, A., Molla, G., Madad, S., Fernandez-Granda, C., and Satija, R. (2024). Dictionary learning for integrative, multimodal and scalable single-cell analysis. Nat. Biotechnol. *42*, 293–304. https://doi.org/10.1038/s41587-023-01767-y.

95. Korsunsky, I., Millard, N., Fan, J., Slowikowski, K., Zhang, F., Wei, K., Baglaenko, Y., Brenner, M., Loh, P.R., and Raychaudhuri, S. (2019). Fast, sensitive and accurate integration of single-cell data with Harmony. Nat. Methods *16*, 1289–1296. https://doi.org/10.1038/s41592-019-0619-0.

96. Miller, B.C., Sen, D.R., Al Abosy, R., Bi, K., Virkud, Y.V., LaFleur, M.W., Yates, K.B., Lako, A., Felt, K., Naik, G.S., et al. (2019). Subsets of exhausted CD8+

T cells differentially mediate tumor control and respond to checkpoint blockade. Nat. Immunol. *20*, 326–336. https://doi.org/10.1038/s41590-019-0312-6.

97. Xu, S., Hu, E., Cai, Y., Xie, Z., Luo, X., Zhan, L., Tang, W., Wang, Q., Liu, B., Wang, R., et al. (2024). Using clusterProfiler to characterize multiomics data. Nat. Protoc. *19*, 3292–3320. https://doi.org/10.1038/s41596-024-01020-z.

98. Gohlke, J.H., Lloyd, S.M., Basu, S., Putluri, V., Vareed, S.K., Rasaily, U., Piyarathna, D.W.B., Fuentes, H., Rajendiran, T.M., Dorsey, T.H., et al. (2019). Methionine-Homocysteine Pathway in African-American Prostate Cancer. JNCI Cancer Spectr. *3*, pkz019. https://doi.org/10.1093/jncics/pkz019.

99. Vantaku, V., Dong, J., Ambati, C.R., Perera, D., Donepudi, S.R., Amara, C.S., Putluri, V., Ravi, S.S., Robertson, M.J., Piyarathna, D.W.B., et al. (2019). Multi-omics Integration Analysis Robustly Predicts High-Grade Patient Survival and Identifies CPT1B Effect on Fatty Acid Metabolism in Bladder. Clin. Cancer Res. *25*, 3689–3701. https://doi.org/10.1158/1078-0432.CCR-18-1515.

100. Putluri, N., Shojaie, A., Vasu, V.T., Vareed, S.K., Nalluri, S., Putluri, V., Thangjam, G.S., Panzitt, K., Tallman, C.T., Butler, C., et al. (2011). Metabolomic Profiling Reveals Potential Markers and Bioprocesses Altered in Bladder Cancer Progression. Cancer Res. *71*, 7376–7386. https://doi.org/10.1158/0008-5472.CAN-11-1154.

101. Yu, W., Chen, Y., Putluri, N., Coarfa, C., Robertson, M.J., Putluri, V., Stossi, F., Dubrulle, J., Mancini, M.A., Pang, J.C., et al. (2020). Acquisition of Cisplatin Resistance Shifts Head and Neck Squamous Cell Carcinoma Metabolism toward Neutralization of Oxidative Stress. Cancers *12*, 1670. https://doi.org/10.3390/cancers12061670.

102. Vantaku, V., Putluri, V., Bader, D.A., Maity, S., Ma, J., Arnold, J.M., Rajapakshe, K., Donepudi, S.R., von Rundstedt, F.-C., Devarakonda, V., et al. (2020). Epigenetic loss of AOX1 expression via EZH2 leads to metabolic deregulations and promotes bladder cancer progression. Oncogene *39*, 6265–6285. https://doi.org/10.1038/s41388-019-0902-7.

103. Cox, A.R., Chernis, N., Bader, D.A., Saha, P.K., Masschelin, P.M., Felix, J.B., Sharp, R., Lian, Z., Putluri, V., Rajapakshe, K., et al. (2020). STAT1 Dissociates Adipose Tissue Inflammation From Insulin Sensitivity in Obesity. Diabetes *69*, 2630–2641. https://doi.org/10.2337/db20-0384.

104. Anders, S., and Huber, W. (2010). Differential expression analysis for sequence count data. Genome Biol. *11*, R106. https://doi.org/10.1186/gb-2010-11-10-r106.

105. Pang, Z., Lu, Y., Zhou, G., Hui, F., Xu, L., Viau, C., Spigelman, A.F., MacDonald, P.E., Wishart, D.S., Li, S., and Xia, J. (2024). MetaboAnalyst 6.0: towards a unified platform for metabolomics data processing, analysis and interpretation. Nucleic Acids Res. *52*, W398–W406. https://doi.org/10.1093/nar/gkae253.